ABSTRACT

AN OPTIC FIBER SENSOR FOR PARTIAL DISCHARGE ACOUSTIC DETECTION

by
Xiaodong Wang

Partial discharge (PD) is a very common problem in operating power transformers and is one of the factors that could lead to failure of power transformers, leading to power outage and expensive repairs. The acoustic wave induced by PD can be measured and used for monitoring, diagnosing, and locating potential failures in power transformers.

The effects of the temperature of the transformer and transformer oil are one of the very important parameters in PD and these effects are investigated in detail. The Fast Fourier Transform (FFT) is used to synthesize the measured data and results show that for periodic PD events, the dominant components of the energy of the PD shift to higher frequencies as the temperature increases. The experimental results are consistent with theoretical expectations.

Fiber optic-based sensors have been shown to be attractive devices for PD detection because of a number of inherent advantages including small size, high sensitivity, electrical nonconductivity, and immunity to electromagnetic interference (EMI). A fiber optic sensor based on a Fabry-Perot interferometry is constructed by a simple micromachining process compatible with MEMS (Microelectromechanical system) technology. The sensor is used in a transformer to measure PD acoustic waves. The experimental results show that the sensor not only has an inherent high signal to noise capability, but is able to accurately localize the PD sources inside the transformer.

AN OPTIC FIBER SENSOR FOR PARTIAL DISCHARGE ACOUSTIC DETECTION

by

Xiaodong Wang

A Dissertation
Submitted to the Faculty of
New Jersey Institute of Technology and
Rutgers, the State University of New Jersey-Newark,
in Partial Fulfillment of the Requirements for the Degree of
Doctor of Philosophy in Applied Physics

Federated Physics Department

January 2005

APPROVAL PAGE

AN OPTIC FIBER SENSOR FOR PARTIAL DISCHARGE ACOUSTIC DETECTION

Xiaodong Wang

Dr. Onofrio L. Russo, Dissertation Advisor — Date
Associate Professor of Physics, New Jersey Institute of Technology

Dr. Ken K. Chin, Dissertation Advisor — Date
Professor of Physics, New Jersey Institute of Technology

Dr. Martin Schaden, Committee Member — Date
Assistant Professor of Physics, Rutgers, The state University of New Jersey-Newark

Mr. Harry T. Roman, Committee Member — Date
Senior Technology Development Consultant, Public Service Electric and Gas Company

Dr. Baoqing Li, Committee Member — Date
Research Associate of Applied Physics, New Jersey Institute of Technology

BIOGRAPHICAL SKETCH

Author: Xiaodong Wang

Degree: Doctor of Philosophy

Undergraduate and Graduate Education:

- Doctor of Philosophy in Applied Physics
  New Jersey Institute of Technology, Newark, NJ 2004

- Master of Mechanical and Production Engineering
  Nanyang Technological University, Singapore, 2000

- Bachelor of Mechanical Engineering
  University of Science and Technology, Beijing, China, 1997

Major: Applied Physics

Presentation and Publications:

Xiaodong Wang, Baoqing Li, Zhixiong Xiao, Harry T. Roman, Onofrio L. Russo, Ken Chin, and Kenneth R. Farmer,
"Acoustic Energy Shifting in Different Temperatures of Transformer Oil", accepted by IEEE Power Engineering Society Letters on October 25, 2004.

Xiaodong Wang, Baoqing Li, Zhixiong Xiao, Sanghwui Lee, Harry T. Roman Onofrio L. Russo, Ken Chin, and Kenneth R. Farmer,
"An ultra sensitive optical MEMS sensor for partial discharge detection", accepted by Journal of Micromechanics and Microengineering on November 28, 2004.

Xiaodong Wang, Baoqing Li, Yan Sun, Harry T. Roman, and Kenneth R. Farmer,
"A unique method to design ultra sensitive diaphragm",
The Nanotechnology Conference and Trade Show, March 7-11, 2004, Boston, Massachusetts, U.S.A.

Sanghui Lee, Zhixiong Xiao, Xiaodong Wang, Ken Chin, and Kenneth R. Farmer,
"Simulation and modeling of a bridge-type resonant beam for Corilis true flow sensor",
The Nanotechnology Conference and Trade Show, March 7-11, 2004, Boston, Massachusetts, U.S.A.

Patent:

Kenneth R. Farmer, Harry T. Roman, Xiaodong Wang, and Baoqing Li,
"Online Fiber Optic Sensor for Detecting Partial Discharge and Similar Events in Large Utility Station Transformers",
Submitted on March 5, 2004.

This thesis is dedicated to

我可爱的太太

My wife

王维佳

我挚爱的父母

My parents

蔡鹏飞和王云霞, 王栋华和陆如珍

可敬的哥哥和嫂嫂

My brother and his family

张庆春,郁玉霞和他们给我家带来无限欢乐的儿子

ACKNOWLEDGEMENT

I want to thank my advisors, Dr. Onofrio L. Russo, Dr. Ken K. Chin and the staff of the Microelectronics Research Center for all their help, support and patience.

Special thanks go to Mr. Harry T. Roman and Public Service Electric and Gas Company (PSE&G) for providing the practical technical guidance and financial support for this research. I would also like to thank Dr. Baoqing Li and Dr. Zhixiong Xiao for their continuous help and support.

I thank Dr. Kenneth R. Farmer for getting me interested in this project and would also like to thank Dr. Martin Schaden, my committee member.

Dr. Ronald Kane, the Dean of Graduate Studies, deserves special thanks for his invaluable help over years.

TABLE OF CONTENTS

TABLE OF CONTENTS
(Continued)

TABLE OF CONTENTS
(Continued)

TABLE OF CONTENTS
(Continued)

LIST OF TABLES

LIST OF FIGURES

LIST OF FIGURES
(Continued)

LIST OF FIGURES
(Continued)

LIST OF FIGURES
(Continued)

CHAPTER 1

INTRODUCTION

1.1 General Overview

PD is a short abrupt flow or release of current caused by buildup of the electric field intensity in a limited region. PD in the transformer is a sign of dielectric defects as well as a cause for further degradation of its insulation system and may therefore lead to a failure of the apparatus. PD measurements have been used for many years during acceptance tests of new high voltage apparatuses for uncovering possible construction problems, such as bad design, defects in insulation materials used, or poor workmanship. They have also been used for detecting the deteriorated parts of the insulation in an apparatus under normal operation [1-5].

The primary methods of PD detection are based on the observable electric and acoustic characteristics of the phenomenon. Acoustic PD detection systems are more favorable than electric systems in transformer monitoring. The problem with current acoustic PD detection systems is that the acoustic signal must be observed outside of the transformer tank because there are no developed sensors that can survive the environment of the tank interior and be electrically and chemically neutral. Because the path between a PD and the acoustic sensors includes the wall of the tank, multipath interference can severely limit the accuracy of any positioning system. The interference is caused by the differing acoustic velocity of the wave in the oil and the transformer tank.

Therefore, it would be an enormous advantage if a sensor could be designed to operate within the transformer tank without inhibiting or changing the functionality of the

transformer [6]. Once an internal sensor has been designed, a positioning system must be employed that makes the most efficient use of the received acoustic signals. The location of the PD source within the transformer tank can be determined by measuring the time difference of arrival of the acoustic signal among several sensor positions within the tank.

1.2 Objective of the Study

The objective of the study is to develop a new technology for on-line monitoring of PD inside high voltage (HV) transformers. The technique has been based on detection of the PD pulses by an optical acoustic sensor system installed inside the transformers. The measuring system is computer assisted utilizing the Fast Fourier Transform (FFT) which is used for PD signal spectrum analysis. The PD measurement is implemented directly in the transformer oil, so attenuation of the signals is negligible compared with a measurement outside the transformers.

1.3 Dissertation Outline

PD detection is very important for the safety of HV transformers. In Chapter 2 PD fundamentals and different detection techniques are described with a focus on PD detection and particularly on PD acoustic signal detection. The experimental and theoretical analysis of PD acoustic signals in transformer oil at different temperature is described in Chapter 3. The working principle, design, fabrication and testing of the optical sensor are described in Chapter 4, and the optical sensor application in PD detection is explained in Chapter 5. The work is finally concluded and suggestions for future work are described in Chapter 6.

CHAPTER 2

LITERATURE REVIEW

2.1 Background

Transformers are one of the most important and cost-intensive components of electrical energy supply network. A review of the structure and age of the transformers in service for different utilities shows, that many of the transformers already have reached their design limit. Thus, a replacement of some transformers can hardly be postponed, but the deregulation forces the utilities to save costs. As a consequence, the need and the interest for measures to extend the life span and load optimization of the components of the electrical power supply strongly rose. As the HV device ages, the insulation can breakdown due to mechanical, thermal and electrical stress, resulting in the catastrophic failure of the device.

Therefore, it is important to have a system that is capable of warning device users of potential insulation problems so that they may be repaired during a scheduled shutdown. This is especially the case for PD-measurements, which are known as an adequate and practical tool for diagnosing the actual condition of the insulation, thus without these measurements only incomplete statements about the insulation condition are possible leading finally to an insecure life-risk management. In order to design a system to detect and locate this phenomenon within a HV transformer, it is important to understand why PDs occur and what methods are currently employed to detect and locate PDs. For this purpose, the knowledge about the operation condition of the component is of enormous importance, thus monitoring and diagnostic systems become more and more

indispensable. PD detection is an important tool for monitoring insulation conditions in HV devices in power systems.

2.2 PD Mechanism

The subject of PD which represents an antecedent term that has been commonly applied to them in the past, constitutes a field of endeavor which can be traced back to the beginning of the twentieth century [7-10]. While the study of PD may thus considered as a well developed field, its preeminent importance as a tool for assessing the quality and performance and characteristics of HV transformer has been responsible for sustaining a high level of activity in investigations related to its mechanism, physical and chemical effects, detection and measurements techniques [11-13].

PD in a HV transformer occurs when the electric field in a localized area changes in such a way that a localized current is created. This localized current manifests itself as an electrical pulse that is measurable at the output of the transformer. The most likely sources of PDs can be broken down into three categories: floating components, coronas, and voids. Information on the importance and mechanisms of floating components and coronas in HV transformers can be found in [14]. However, the detection of PDs created by these two sources does not yield any useful information about the insulation because their appearance is not directly related to the condition of the insulation. Insulation breakdown is physically manifested as small cracks, *i.e.* voids, in the insulation; therefore, only void sources will be considered here.

Voids are defined as gaps in a more dense dielectric material, such as gas bubbles in oil that fills the transformer tank, or cracks and fissures in the paper insulation lining

the transformer walls. The void region has a lower dielectric constant than the surrounding material so that PD can occur when the electric field difference across the void exceeds the minimum breakdown field strength. However, reaching this minimum field strength does not guarantee an immediate PD. In order for PD to occur, two criteria must be met. First, the electric field difference across the void must be higher than the breakdown value, which is determined by the field's ability to accelerate an electron to the point that if it impacts another molecule, more electrons are released than are absorbed. Second, the voltage across the void must contain free electrons and the voltage across the specific volume of the void must be proportional to the size of void. If these conditions are met, then the buildup of electrons in motion grows exponentially and a streamer, or electron channel, is created so that current can flow across the void and return the voltage across the void to zero [15].

2.3 PD Detection Methods

2.3.1 Introduction to PD Detection

Occurrence of PDs in electrical insulation is always associated with emission of several signals: electrical and acoustic pulses and chemical reactions. These signals are a means for detection and quantification of PD activities in high voltage apparatuses. Over the past forty years, several methods have been developed to detect PDs within HV transformers. These can be grouped into three categories, based on the PD manifestation that they measure: chemical, electrical, and acoustic detection. Each is briefly explained in the following sections.

2.3.2 Chemical Detection

One of the consequences of PDs is chemical change of material [16-18]. For example, a PD activity in GIS equipment decomposes SF_6 to basic chemical species. This has been exploited to produce a low cost gas analyzer to detect SOF_2 and thereby to detect PD sources. In rotating machines, the presence of ozone in cooling air is evidence of the discharge activity [19].

The two primary chemical tests employed by power companies today are dissolved gas analysis (DGA) [20] and high performance liquid chromatography (HPLC) [21]. The DGA test identifies gas levels in the oil produced by the breakdown of mineral oil in the transformer into different gases, which dissolve back into the oil. The test is administered by taking an oil sample from the tank and determining the levels of different dissolved gases, which include acetylene, methane, hydrogen, carbon dioxide, and ethylene. Another test, HPLC, measures the byproducts of transformer wall insulation breakdown. Because the insulation on the wall of the transformer is made of paper, the breakdown products are glucose and degraded forms of glucose. The test is administered by evaluating oil samples from the transformer in an offsite lab.

Chemical testing has some limitations that prevent it from being the only method used for PD detection. First, chemical testing does not provide any information about the position of the PD or the extent of the insulation damage. The second problem is that chemical testing cannot be performed online. In most cases, the transformers must be taken out of operation to obtain the oil sample. These problems limit the usefulness of chemical detection and rule it out as a singular solution to PD detection and positioning.

2.3.3 Electrical Detection

During a PD a finite amount of charge carriers, electrons and ions, flow between the discharge surfaces in a short time. This results in generation of current and voltage pulses of short rise times that appear across the insulation. Electrical detection focuses on capturing the electrical pulse created by the current streamer in the void. These pulses last on the order of single nanoseconds and have measurable frequency components in excess of 1 MHz [14]. These pulses have been one of the primary means for detection and measurement of PD activity in insulation systems using high frequency current transformers [22-24]. Electromagnetic waves are radiated from the discharges in the RF band, 100 kHz to several hundreds of megahertz. These waves are detectable using proper electromagnetic probes (antennas). The PD is then identified using several digital processing methods. These processing methods make online electrical PD detection very attractive because it makes real-time monitoring of HV systems possible. Using an RF directional antenna the PD site may be localized [25, 26].

Like chemical detection, electrical detection has limitations. The primary limitation of electrical testing is its susceptibility to noise. The HV transformer environment contains high levels of electrical noise, both narrowband and broadband. In some cases, it is extremely difficult to distinguish between noise and a PD because of the short PD pulse width. This problem leads to false detection in online electrical PD systems. The transformer can be taken offline and connected to an external power source for testing in order to eliminate some of the noise, but taking the HV transformer offline can cost hundreds of thousands of dollars a day in lost revenue for the power company [27]. Another problem with electrical detection is that the received pulse characteristics

are highly dependent on the geometry of the HV transformer. Different components within the transformer can distort the pulse shape needed to characterize the type of PD fault and can again result in erroneous detection.

2.3.4 Acoustic Detection

Acoustic detection of PDs is based on the detection of the mechanical waves propagated from the discharge site to the surrounding medium. This signal is created because when the current streamer is formed within the void, the material around the hot streamer is vaporized. This vaporization causes an explosion of mechanical energy, which then propagates through the transformer tank in the form of a pressure field [28-34]. Acoustic detection has been widely used in diagnostics of transformers. In transformers, the use of piezoelectric transducers attached to the transformer tank wall has been the most favored approach [35].

The primary advantage of using acoustic detection over chemical and electrical methods is that position information is readily available from acoustic systems using sensors at multiple locations. This position information can help to identify the type of PD as well as the location and severity of an insulation fault. Acoustic detection has another advantage that observations can be made in the presence of large electromagnetic disturbances.

However, some factors make the detection and interpretation of the results rather complicated. These factors include the complexity of the acoustic impedance between the PD source and the detector, frequency dependent velocity, transmission losses in different media, different velocities for the different transmission types and reflections at impedance discontinuities.

2.4 Acoustic Detection Classifications

This section provides the necessary review of acoustic detection sensors currently in production. PD acoustic detection sensors can be grouped into external and internal monitoring sensors. External PD monitoring employs acoustic sensors located outside of the transformer tank. Internal PD monitoring employs acoustic sensors inside the transformers.

2.4.1 External Detection Sensors

Several different technologies are used to fabricate these external sensors, but piezoelectric transducers based on ferroelectric ceramic materials such as lead zirconium titanate (PZT) dominate the systems currently in use. A PZT sensor converts acoustic energy into an electrical signal.

Since piezoelectric acoustic sensors have wide bandwidth, are smaller than coupling capacitors, and are capable of being inserted into the oil, or measuring acoustic signals at transformer walls, they have been used in PD detection. Two types are used in acoustic detection, accelerometers and acoustic emission sensors. Accelerometers, which have a useful frequency range of up to 50 kHz, produce an electrical signal that is proportional to the acceleration of the surface that the sensor is connected to. In contrast, acoustic emission sensors, with a frequency range between 30 kHz and 1 MHz, produce an electrical signal that is proportional to the velocity of the contact surface [36].

Both types of sensors are considered acoustic-electric (AE) sensors because they convert mechanical vibrations into a corresponding electrical signal. Because the electrical noise [37-38] environment of the HV transformer is so severe, the signal to noise ratio at the output of the AE sensor can be significantly reduced. Sensors and

receiver equipment are shielded to lower their susceptibility to EMI, but are not completely immune. The position accuracy of these systems fall within useful bounds, but the time it takes to find the position is much too long. Because PD can cause a failure in minutes or in hours, it is desirable for the results to be instantaneous or at least available in quasi-real time. One of the reasons that these calculations take so long is due to multipath interference. The sensors for the acoustic detection system are located outside the tank. The acoustic pulse can take several different paths along the transformer interior and exterior to reach the sensor. Therefore, the same portion of the pulse can arrive at the same sensor at different times. This effect is exacerbated by the fact that the acoustic wave travels faster in the steel walls than in the fluid medium. While multipath effects can be removed, it requires multiple measurements of the PD as well as a large amount of computation time to accomplish. This speed limitation is one of the primary drawbacks of the external measurement systems. The multipath issue can be circumvented if the sensors are placed within the transformer tank. Internal systems have the advantage of measuring the acoustic wave directly from the liquid medium before reflection and multipath can distort the signal [39]. The problem with internal systems is that AE sensors cannot be placed within the transformer tank because they transmit an electrical signal that can interfere with the workings of the transformer. New acoustic sensor technologies that are suitable for the harsh environment of an HV transformer must be developed.

2.4.2 Internal Detection Sensors

PD occurring in oil produces a pressure wave that is transmitted throughout the transformer via the oil medium. The new technology, fiber optic sensing, is making it possible for acoustic sensors to be placed inside the HV transformer. Fiber optic technology is ideal for this application because the devices are chemically and electrically inert. Therefore the sensor can be placed within the HV transformer tank where sensors operate at frequencies of 100 to 300 kHz with a resonance frequency of 150 kHz. Also, because the fiber sensor uses an optical signal to measure acoustic waves, the sensor is completely immune to EMI. There are several interferometer-based designs for fiber optic acoustic sensors [40-43], but the sensitivities of these sensors are not high. In the following chapters, an optic fiber sensor development for PD acoustic detection is described in detail. Table 2.1 shows the PD detection comparisons between external detection (using PZT acoustic sensor) and internal detection (using optic fiber sensor).

Table 2.1 Comparisons of PD Measurement Methods.

	Advantages	**Disadvantages**
PZT Acoustic Sensor	Has high voltage limits, but low stiffness and electromechanical coupling coefficient Wide working range High sensitivity Low cost Simple interface circuit	Low temperature range Ineffective in high frequency noise environments Piezo material is brittle, care to be taken during installation and use to prevent breakage
Fiber Optical Acoustic Sensor	Small size Wide temperature range High sensitivity Immunity to EMI Immunity to inner chemical medium electrically passive Can be "snaked" close to PD source	Still in very early stage of development Relatively complex interface circuit Difficult to fabricate without the right facilities (such facilities are present at NJIT)

2.5 Discussions and Conclusions

PD is an electrical phenomenon that causes insulation deterioration and frequently is the reason for breakdown (failure) of an insulation system. Most incipient dielectric failures generate PD prior to complete failure. Sometimes the failure occurs within a matter of minutes or hours after the inception of PD; but in other cases PD activity can be present for years. It is therefore vital that PD measurements be made in the field in order to predict these abnormal conditions [44-46].

One can achieve acoustic PD detection by mounting piezoelectric acoustic sensors externally on the walls of a power transformer. An externally mounted piezoelectric acoustic sensor offers the advantages of easy installation and replacement. However, a piezoelectric sensor may suffer from degeneration of the signal-to-noise ratio caused by environmental noises such as EMI and corona effects. Another possible disadvantage associated with an externally mounted piezoelectric sensor is that the multiple paths of acoustic wave transmission make locating the exact positions of PDs difficult.

It is thus desirable to have sensors that can function reliably inside a transformer, even deep within the transformer windings, to pick up clean PD-induced acoustic signals. For the sake of safety and easy installation these sensors have to be chemically inert, electrically nonconducting, passive, and small in size.

Optical fiber-based sensors have been shown to be attractive devices with which to measure a wide range of physical and chemical parameters because the sensors have a number of inherent advantages, including small size, light weight, high sensitivity, high frequency response, electrical nonconductivity, and immunity to EMI noise. It can be used for in-oil detection of PD and "snaked" close to the source via available openings in the transformer like oil drain plugs. These advantages make optical fiber sensors excellent candidates for PD detection.

CHAPTER 3

ACOUSTIC SIGNALS IN TRANSFORMER OIL AT DIFFERENT TEMPERATURES

3.1 Introduction

Considerable research has been expended in the development of field techniques for PD detection and measurement. An acoustic emission technique is useful to detect PD in which sound and ultrasound waves are observed as elastic waves by a piezoelectric acoustic sensor [47-50].

The importance of the temperature of transformer oil in the analysis of PD acoustic spectrum has not been previously investigated. In this chapter, acoustic waves at temperatures of 25°C and 40°C have been measured and the measurements results are analyzed by means of the Fast Fourier Transform (FFT). The experimental results show that the dominant frequency components in the energy of the PD pulse shift from low frequency to high frequency at increased temperature. A theoretical analysis is shown to be consistent with the experimental results.

3.2 Experimental Setup

Acoustic sensors are available for a variety of frequency ranges from 30 kHz to several MHz, which are far above most of the background noise, but are low enough to give good detection ranges in most applications in transformers. Usually they are manufactured from piezoelectric ceramics or piezoelectric crystal. Since piezoelectric acoustic sensors have wide bandwidth and can measure acoustic signals when placed on transformer walls, they have been used in PD detection. In this experiment a Harisonic G-0504 type

piezoelectric sensor is used, with frequency response up to 5 MHz, well above the expected PD acoustic signal frequency of 400 kHz.

The PD generator circuit is shown in Figure 3.1. As illustrated in the block diagram in Figure 3.2, the circuit of Figure 3.1 accomplishes three tasks: 1) first it converts a low DC voltage of about 5 V, to a high AC voltage, 2) it then charges a capacitor at a high voltage, and 3) it discharges the capacitor when the switch is closed generates a PD between two needles with approximately 0.5 mm apart. A voltage gain factor of the circuit is about 2000. Figure 3.3 shows the fabricated PD generator.

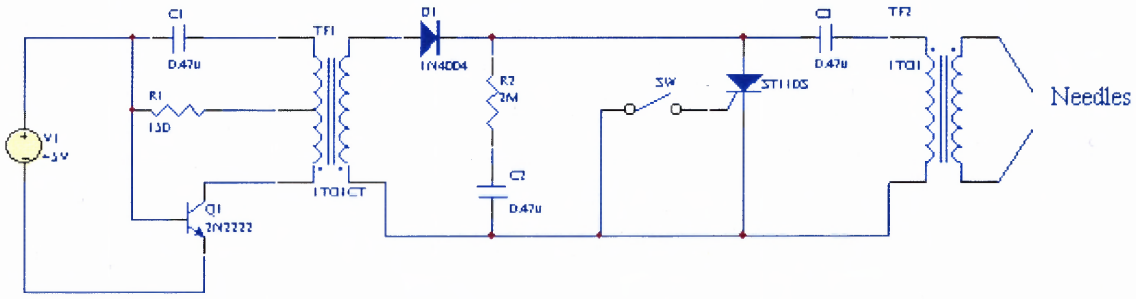

Figure 3.1 PD generator circuit design.

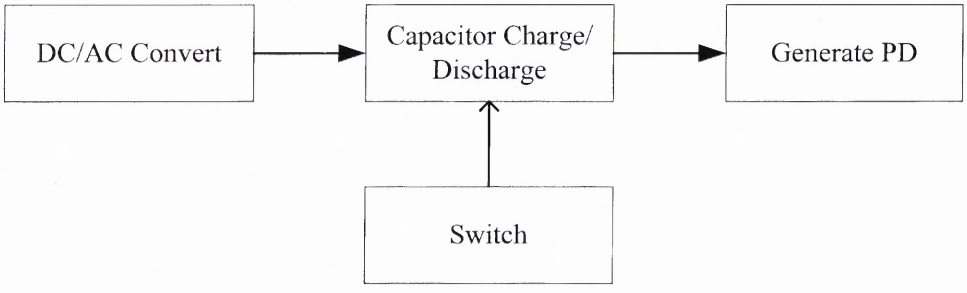

Figure 3.2 The working principle of the PD generator circuit.

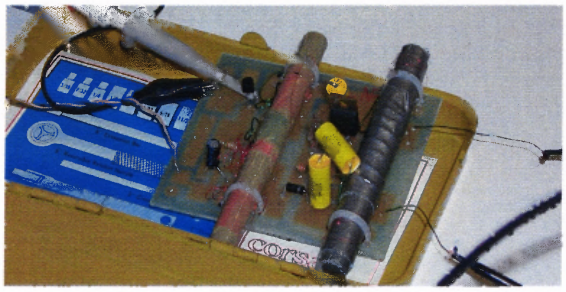

Figure 3.3 Fabricated PD generation circuits.

Figure 3.4 shows a close-up of the spark tank, spark gap and assembly. The spark tank consists of a plastic tub filled with transformer oil, two micromanipulators for placing and holding opposing electrodes in close proximity, and two hypodermic needles to serve as sharp electrodes. The needle electrodes have a diameter of 0.1mm. The gap length between the needles is 0.5 mm. An air compressor is used to create a source of bubble in the vicinity of the spark gap. Sparks are generally modeled as occurring across a bubble in the oil. Figure 3.5 shows the test apparatus (left to right): low noise Ithaco amplifier connected to the piezoelectric sensor, a digital oscilloscope (HP Model 54616C) with sampling frequency of 500 MHz connected to the amplifier and 5 V DC power supply connected to the spark generator circuit.

The piezoelectric sensor detects PD sounds in the transformer oil and transfers it to the oscilloscope for real time display and storage. Then the data is sent to a computer for FFT analysis.

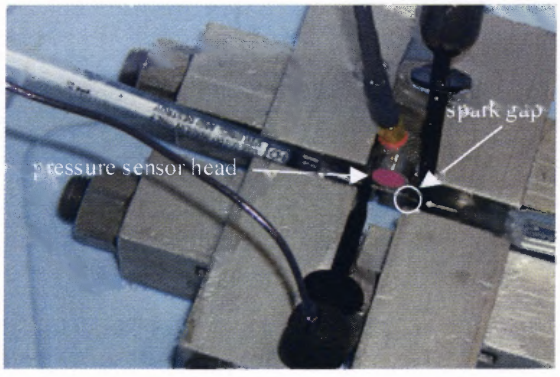

Figure 3.4 A close-up of the spark tank, spark gap and assembly.

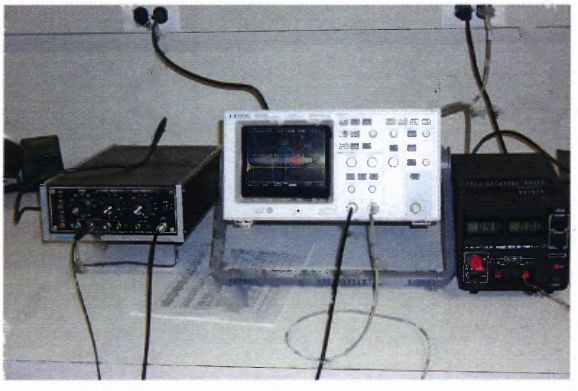

Figure 3.5 PD detecting test apparatus.

3.3 Experimental Results

In this section, PD detections in air and transformer oil are detected and analyzed. PD signals are also studied at different temperatures. In order to simplify the analysis of the experimental results, all experiments are carried out using the same needle gap in the transformer oil, and all acoustic signals are detected at the same distance between needles and the acoustic sensor.

3.3.1 Spark Detection in Air

A typical oscilloscope image is presented in Figure 3.6 showing the acoustic signature of a spark in air (upper trace). In each of the oscilloscope images in this section, the upper trace is the amplified transducer output curve and the lower trace is measured within the spark generator circuit. Thus the upper trace is the only data of interest. The curve displays two distinct regions, an initial very noisy period beginning less than 0.1 division (about 2.0 μs) from the start of the data, lasting for about 20 μs (about 1 division), and a second lower frequency noisy region beginning at t = 20 μs on the trace. The first region is EMI pick-up due to the spark and provides an accurate measure of the initial onset of the spark. The second region is the acoustic pick-up of the transducer (think of this as the thunder heard some time after the lightening flash), and is displaced from the initial onset of the spark because of the finite speed of sound, i.e., the pressure sensor head is displaced some distance (in this case about 7 mm) from the spark sound source. The shape of the sound pulse is found to be fairly repeatable from spark to spark, generally consisting of a large amplitude pulse followed by smaller amplitude features. The duration of the single large amplitude pulse (about 15 μs) corresponds to a "frequency" of about 65 kHz, lower than the 200 kHz expected for oil. Since the spark is audible to the ear, it contains frequency components that are less than 20 kHz.

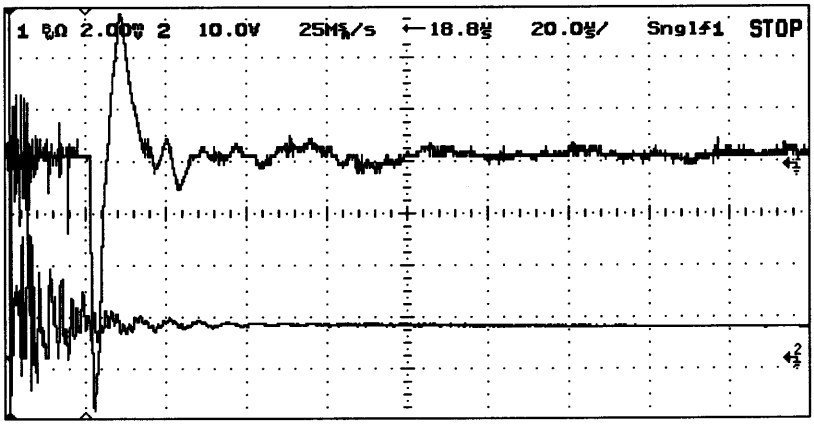

Figure 3.6 The upper trace is the acoustic signature of a spark in air with the sensor roughly 7 mm away from the spark source.

The upper trace in Figure 3.7 shows the sensor response measured with the transducer placed roughly 35 mm from the spark sound source. Observe that the initial large amplitude pulse is attenuated, compared to the 7 mm measurement, as one would expect for sound radiating in all directions. The significant attenuation will require phase-lock loop (PLL) or other detections for applications that are far removed from a quiet sound source in air. Also notice in the figure that the pulse is farther displaced from the EMI initial onset region, indicating that the sound takes longer to travel the greater distance through the air from the spark sound source to the sensor head. By measuring the time of flight versus distance one can calculate the speed of sound in air. In Figures 3.6 and 3.7 the speed of sound in air is approximately 350 m/s (around 7mm/20μs and ~35mm/100μs, respectively), as expected.

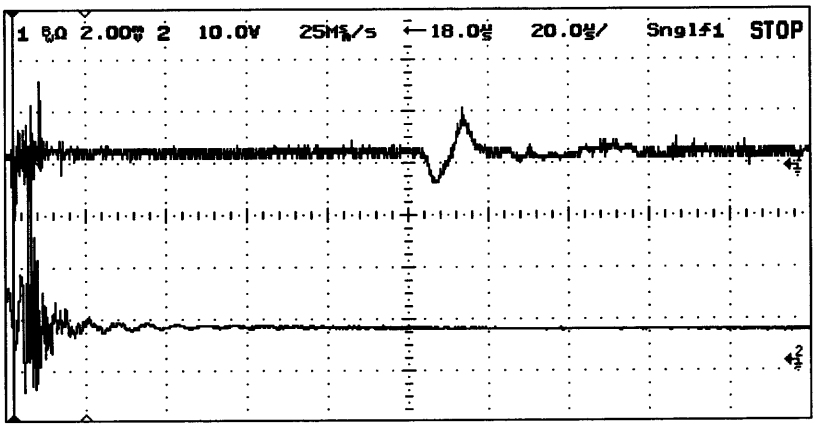

Figure 3.7 The upper trace is the acoustic signature of a spark in air with the sensor roughly 35 mm away from the spark source.

3.3.2 Spark Detection in Transformer Oil

Figure 3.8 shows a typical acoustical signature of a spark in transformer oil. In this case, the sensor is located roughly 30 mm from the sound source. In the figure there are several observations of interest including

- The initial 15 μs acoustic pulse is not as dominant in oil as it is in air,
- The high frequency components of the signal may be 200 kHz (0.25 divisions), but there are clearly lower frequency components as well,
- While the electromagnetic noise due to the light of the spark lasts only approximately 20 μs, the acoustic signal persists for at least 4 divisions or 80 μs before repeating itself.

After some investigation, it is determined that the repeated signal is merely an echo of the initial 80 μs sound signature, most likely reflected from a wall of a micromanipulator. This suggests that the sound features in the initial portion are due to the spark and not themselves echoes. This persistence is a striking observation that bears further investigation. It may be analogous to the rumble of thunder that persists

significantly longer than the flashes of lightening. If a dominant frequency component within this persistent signal repeats for five or more cycles, it may provide an opportunity for PLL detection.

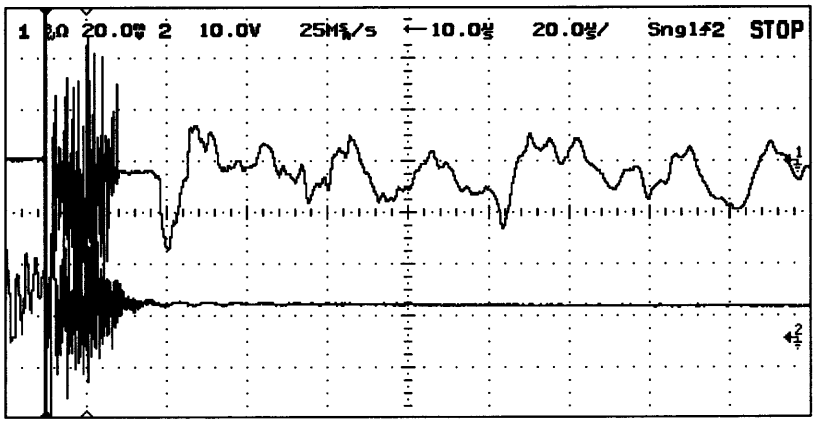

Figure 3.8 The upper trace is the acoustic signature of a spark in oil with the sensor roughly 30 mm away from the spark source.

Figures 3.9 and 3.10 shows the same sparking in oil, but measured at increasing distances from the spark sound source, 50 mm and 75 mm, respectively. In each case, the wave train repeats itself after roughly 4 divisions, and the signals in all three figures look fairly similar in structure. Also, attenuation is observed with increasing distance from the sound source, but the persistence of the wave train is still notable, and the attenuation may be less than that in air.

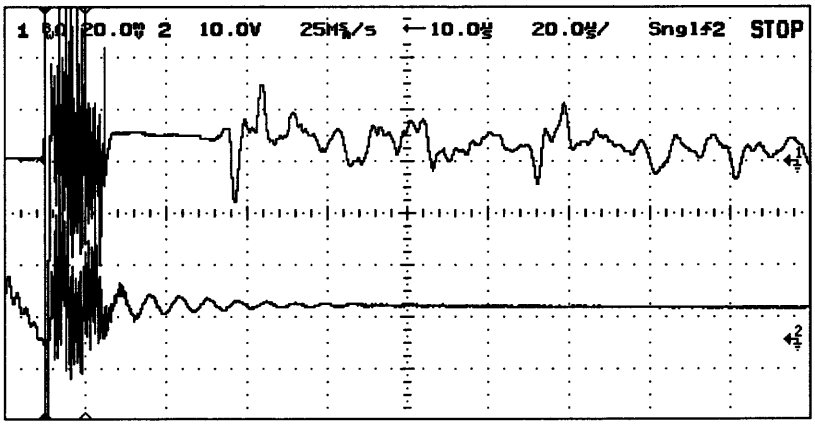

Figure 3.9 The upper trace is the acoustic signature of a spark in oil with the sensor roughly 50 mm away from the spark source.

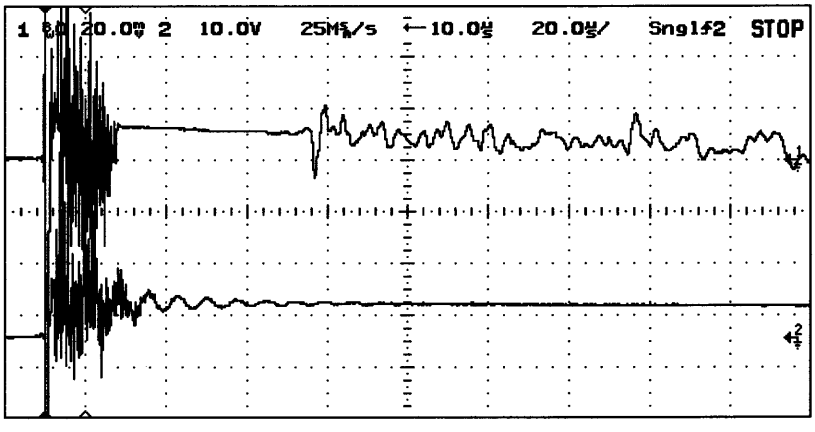

Figure 3.10 The upper trace is the acoustic signature of a spark in oil with the sensor roughly 75 mm away from the spark source.

The data in Figures 3.8, 3.9 and 3.10 give an average value for the speed of sound in oil of about 1,440 m/s (30mm/20μs, 50mm/35μs and 75mm/52μs, respectively), significantly higher than that in air, as expected [51]. The graphical speed of sound derivations for both air and oil are shown in Figure 3.11. The calculated regression slope values give the speed of sound in mm/μs. The average sound velocity is around 350 m/s in air and 1440 m/s in transformer oil [52].

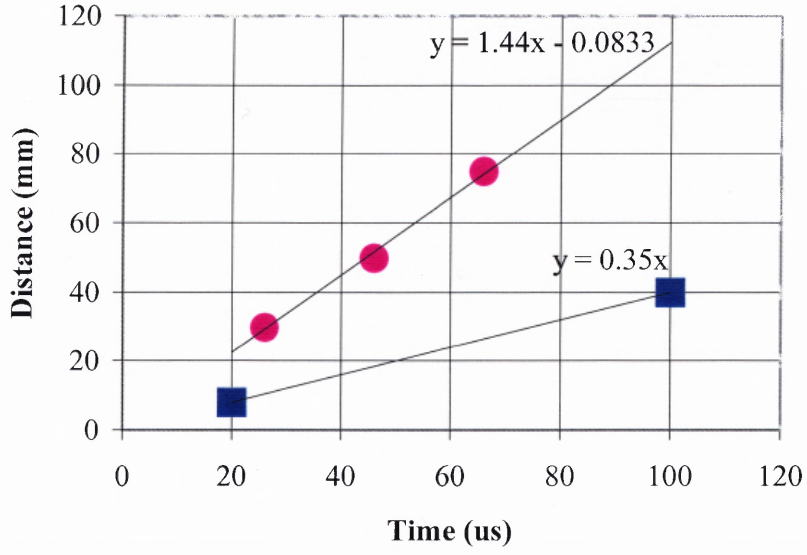

Figure 3.11 Distance-time plot for sound in air (squares) and oil (circles).

3.3.3 Acoustic Signals at Different Temperatures

A typical sound signal for a spark in oil at 25°C is shown in Figure 3.12 with the sensor 5 cm away from the spark. The signal is reproducible from spark to spark in a given medium at a given temperature. This is illustrated in Figure 3.13 that shows 25 spark traces in oil. In Figure 3.13 similar sound signatures are observed for each spark (the curves overlap), indicating that the character of the signal can be spectrally analyzed.

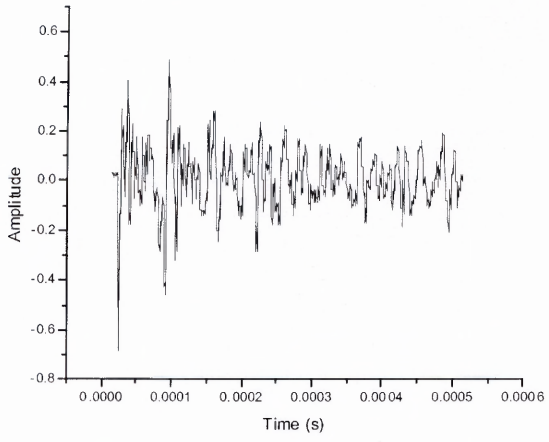

Figure 3.12 Single typical spark wave at 25 degrees C.

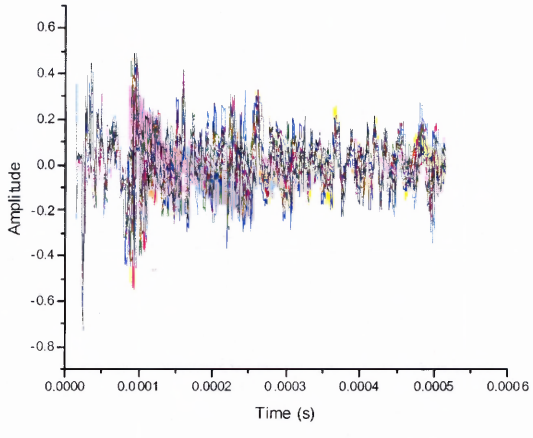

Figure 3.13 Twenty-five periodic spark wave at 25 degrees C.

Spectral analysis is performed by digitizing the sound signal, then fast Fourier transforming the result into the frequency domains. Figure 3.14 is a set of FFT of 25 spark time traces in transformer oil at 25 degrees C. The figure shows that, owing to their similarity in the time domain, sparks emit sound at fairly reproducible frequencies. This is not unexpected since the underlying physics that gives rise to each set of spark

sounds is well defined, if not well understood. The similarity between sparks indicates that "smart" sensing, enabled by analytical software, can be used to detect PD signals by listening for the characteristic signature of the sound.

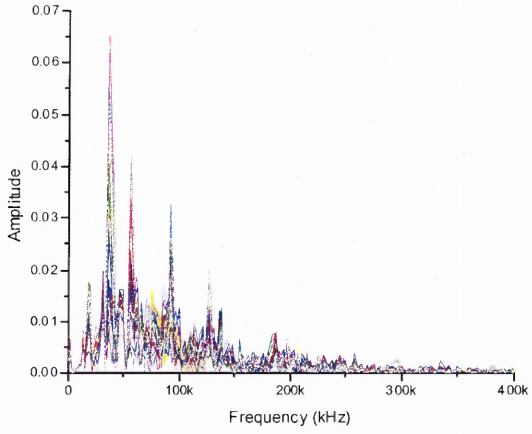

Figure 3.14 FFT results of 25 periodic spark time traces at 25 degrees C.

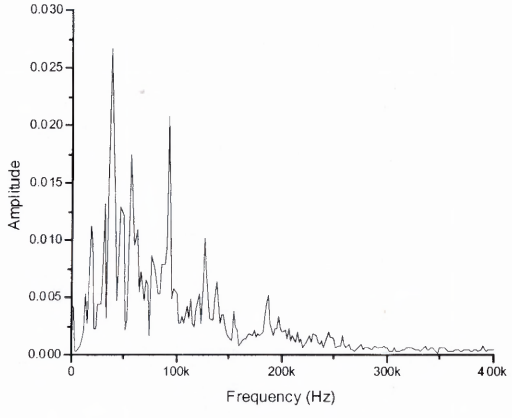

Figure 3.15 The average of FFT results of 25 periodic spark time traces at 25 degrees C.

Figure 3.15 shows the average FFT analysis result for 25 spark time traces. Since the "energy" transported by a wave is proportional to the square of its amplitude, Figure 3.16 shows the relationship between frequency and energy at 25 degrees C. Figure 3.17

shows the spectral energy of discharge in transformer oil at 40 degrees C. Figure 3.16 and 3.17 shows that most of the energy is distributed in 0-100 kHz ranges and very little in the 200-400 kHz ranges.

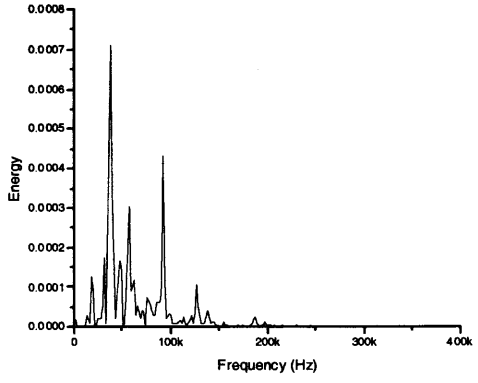

Figure 3.16 Frequency spectrums for energy at 25 degrees C.

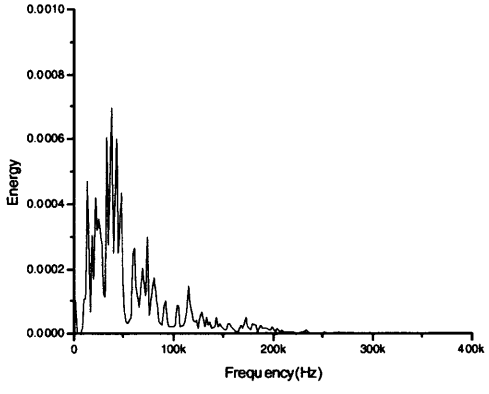

Figure 3.17 Frequency spectrums for energy at 40 degrees C.

By integrating over 50 kHz regions, one can smooth the FFT plots and focus on the increased energy at higher frequencies at higher temperatures. Figure 3.18 shows these integration results along with Table 3.1 of the calculated data which shows the normalized energy in different parts of frequencies at two temperatures. According to the

table, the percentage at 40°C is larger than at 25°C when the frequency is greater than 100 kHz. Clearly energy is shifted from the low to high frequencies with increased temperature.

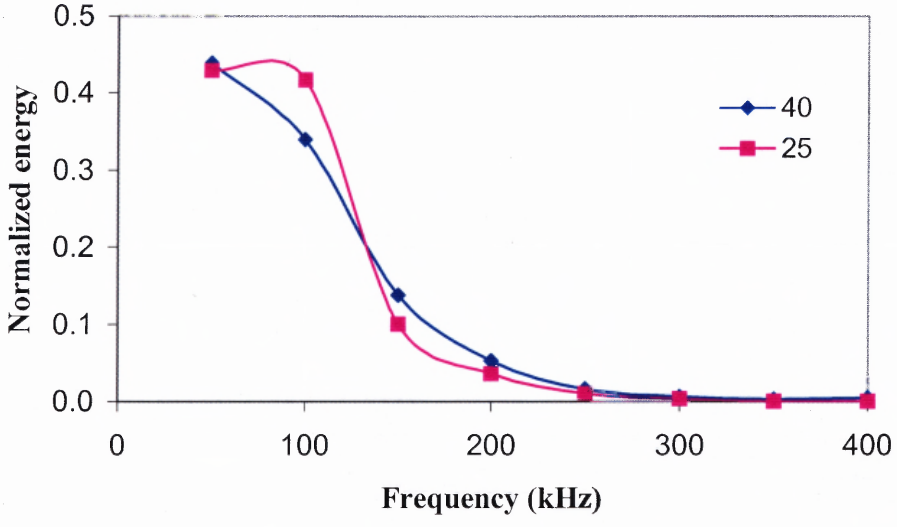

Figure 3.18 The energy integration results at 25 and 40 degrees C

Table 3.1 Experimental Normalized Energy and Ratio at 25 and 40 Degrees C.

Frequency (Hz)	25°C	40°C	Ratio
0 - 50k	42.91%	43.83%	1.02
50k - 100k	41.68%	33.95%	0.81
100k - 150k	10.09%	13.76%	1.36
150k - 200k	3.64%	5.34%	1.47
200k - 250k	1.11%	1.63%	1.47
250k - 300k	0.40%	0.68%	1.7
300k - 350k	0.09%	0.33%	3.67
350k - 400k	0.08%	0.48%	6

3.4 Theoretical Analysis

PD acoustic waves are longitudinal waves due to the characteristics of transformer oil (viscid fluid medium). And acoustic wave propagation speed in transformer oil is about 1440 m/s under normal conditions. The acoustic waves in the oil-filled transformer can be treated as linear wave propagation.

The sources of the acoustic wave dissipation may be divided into two general categories: those intrinsic to the medium and those associated with the boundaries of the medium. Losses in the medium may be further subdivided into three basic types: viscous loss, heat conduction losses and losses associated with internal molecular processes. It is proven that the most of energy loss is associated with viscous losses. So only the viscous affect will be discussed in the wave equation derivation.

3.4.1 Acoustic Wave Propagation

Assuming the fluid is adiabatic, homogenous, and isotropic; the viscous wave equation is shown as following [53]:

$$\frac{4\nu}{3c_0^2} p_{xxt} + p_{xx} - \frac{1}{c_0^2} p_{tt} = 0 \tag{3.1}$$

To simplify the notation, subscipts (t and x) are used to represent the derivative of the function respective to time and/or distance. Where ν is the kinetic viscosity coefficient, c_0 is the acoustic wave propagation velocity in the medium. Then Equation 3.1 can be shown as following:

$$\frac{4\nu}{3c_0^2} \nabla p_t + \nabla^2 p - \frac{1}{c_0^2} p_{tt} = 0 \tag{3.2}$$

Let $p = p_0 e^{j(\omega t - k \cdot x)}$, then

$$p_{xxt} = p_0(-k^2 j\omega) e^{j(\omega t - k \cdot x)} \tag{3.3}$$

$$p_{xx} = p_0(-k^2) e^{j(\omega t - k \cdot x)} \tag{3.4}$$

$$p_{tt} = p_0(-\omega^2) e^{j(\omega t - k \cdot x)} \tag{3.5}$$

Insert the above three derivatives into Equation 3.1 and eliminating the constant and the common exponential terms,

$$\left(1+j\frac{4\nu\omega}{3c_0^2}\right)k^2-\frac{\omega^2}{c_0^2}=0 \tag{3.6}$$

Then

$$k^2=\frac{\omega^2}{c_0^2}\left(\frac{1}{1+j\dfrac{4\nu\omega}{3c_0^2}}\right)=\frac{\omega^2}{c_0^2}\frac{1}{1+\left(\dfrac{4\nu\omega}{3c_0^2}\right)^2}-j\frac{\omega^2}{c_0^2}\frac{\dfrac{4\nu\omega}{3c_0^2}}{1+\left(\dfrac{4\nu\omega}{3c_0^2}\right)^2} \tag{3.7}$$

Let $k=\pm(\beta-j\alpha)$

$$\beta^2-\alpha^2=\frac{\omega^2}{c_0^2}\frac{1}{1+\left(\dfrac{4\nu\omega}{3c_0^2}\right)^2}=A$$

$$2\alpha\beta=\frac{\omega^2}{c_0^2}\frac{\dfrac{4\nu\omega}{3c_0^2}}{1+\left(\dfrac{4\nu\omega}{3c_0^2}\right)^2}=B$$

Where

$$\beta^2 = \frac{1}{2}\left(\sqrt{A^2 + B^2} + A\right)$$

$$\alpha^2 = \frac{1}{2} - \left(\sqrt{A^2 + B^2} + A\right)$$

Then

$$\beta^2 = (\frac{\omega}{c_0})^2 \frac{1}{2}\left[\frac{1}{1+\left(\frac{4\nu\omega}{3c_0^2}\right)^2} + \frac{1}{\sqrt{1+\left(\frac{4\nu\omega}{3c_0^2}\right)^2}}\right]$$

$$\alpha^2 = (\frac{\omega}{c_0})^2 \frac{1}{2}\left[\frac{1}{\sqrt{1+\left(\frac{4\nu\omega}{3c_0^2}\right)^2}} - \frac{1}{1+\left(\frac{4\nu\omega}{3c_0^2}\right)^2}\right]$$

$$\alpha\beta = (\frac{\omega}{c_0})^2 \frac{1}{2} \frac{\frac{4\nu\omega}{3c_0^2}}{1+\left(\frac{4\nu\omega}{3c_0^2}\right)^2}$$

$$\alpha = \frac{1}{2} \frac{\omega^2 \frac{4\nu}{3c_0^3}}{1+\left(\frac{4\nu\omega}{3c_0^2}\right)^2}$$

When $\left(\frac{4\nu\omega}{3c_0^3}\right)^2 << 1$, then

$$\alpha \approx \frac{1}{2}\omega^2 \frac{4\nu}{3c_0^3} = \frac{\omega^2\nu}{6c_0^3} \tag{3.8}$$

The time –harmonic solution of pressure becomes

$$p = p_0 e^{j(\omega t - \beta x + j\alpha x)}$$

$$p = p_0 e^{-\alpha x} e^{j(\omega t - \beta x)} \tag{3.9}$$

The magnitude of the attenuation coefficient ($\alpha \approx \frac{\omega^2\nu}{6c_0^3}$) determines how fast the peak amplitude of $e^{j(\omega t - \beta \cdot x)}$ decays. The attenuation coefficient is related with viscosity and velocity. In normal condition, the velocity is a constant. It is necessary to consider the effect of viscosity in the medium. Since viscosity is temperature dependent, it is important to investigate the effect of temperature in acoustic wave traveling.

3.4.2 Theoretical Calculation

One can perform theoretical analysis on traveling waves in oil to calculate what one would expect for the temperature dependence of sound transport. The amplitude of a traveling sound wave in oil is:

$$P(x,t) = P_0 e^{-\alpha x} e^{i(\omega t - \beta \cdot x)} \tag{3.10}$$

Where $\alpha = \frac{\omega^2 \nu}{6c_0^3}$ and $\omega = 2\pi f$, Equation 3.10 becomes

$$P(x,t) = P_0 e^{\frac{-(2\pi f)^2 \nu}{6c_0^3} x} e^{i(\omega t - \beta \cdot x)} \tag{3.11}$$

In the experiments, the transformer oil (76 Lubricants Company) is used. The viscosity of the oil is shown in Table 3.2 [54].

Table 3.2 Viscosity of Transformer Oil at Different Temperatures.

Viscosity / Temperature	Unit (cSt)
0°C	66
40°C	9.1
100°C	2.6

Since viscosity is temperature dependent, the relationship between viscosity and temperature can be expressed by Equation 3.12 [55]:

$$\nu = \frac{\nu_0}{1 + a(T - 273.15) + b(T - 273.15)^2} \tag{3.12}$$

In Equation 3.12, a and b are constants determined from 2 temperature-viscosity points, which are commonly 40 °C and 100 °C. v_0 (unit cSt) is kinetic viscosity at 0°C. One cSt is 10^{-6} m^2/s. According to Table 3.2, a is 0.097965 and b 0.0014588. The relationship between temperature and viscosity for the oil is shown in Figure 3.19.

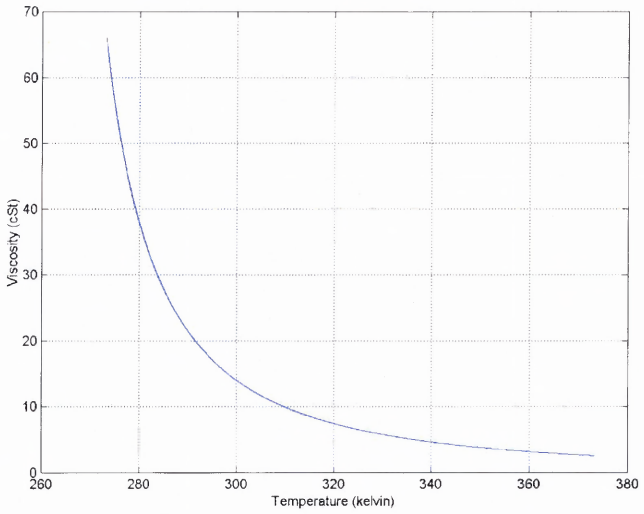

Figure 3.19 The relationship between transformer oil viscosity and temperature.

Since viscosity is temperature dependent, Equation 3.12 becomes:

$$P(x,t) = P_0 e^{\frac{-(2\pi f)^2 v_0}{6c_0^3\left(1+a(T-273.15)+b(T-273.15)^2\right)}x} e^{i(\omega t-\beta\cdot x)} \qquad 3.13$$

The amount of energy carried by a wave is related to the amplitude of the wave. Considering a sound wave, the amplitude of the wave is synonymous with the pressure amplitude. A high-energy wave is characterized by a high amplitude. The energy

transported by a wave is directly proportional to the square of the amplitude of the wave. Since the amplitude of the wave is

$$P_0 e^{\frac{-(2\pi f)^2 \nu_0}{6c_0^3\left(1+a(T-273.15)+b(T-273.15)^2\right)}x} \tag{3.14}$$

The "energy" transported by a wave is proportional to the square of its amplitude:

$$\left(P_0 e^{\frac{-(2\pi f)^2 \nu_0}{6c_0^3\left(1+a(T-273.15)+b(T-273.15)^2\right)}x} \right)^2 \tag{3.15}$$

Since the distance between the sensor and needle is fixed, x is a constant in Equation 3.13. One can smooth the FFT plots and focus on the increased energy at higher frequencies at higher temperatures. Figure 3.20 shows these integration results. Table 3.3 shows that the ratios increase with increased frequencies. Clearly energy is shifted from the low to high frequencies at the higher temperature.

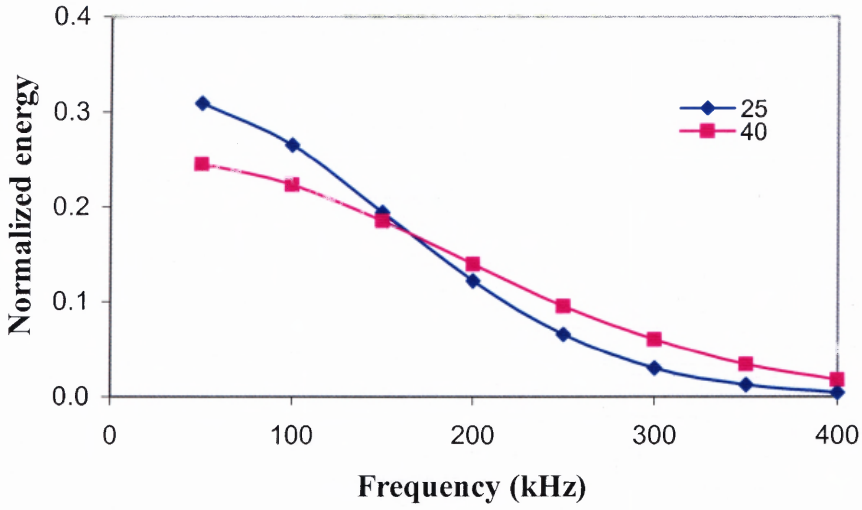

Figure 3.20 Frequency spectrums for theoretical normalized energy.

Table 3.3 Theoretical Normalized Energy and Ratio at 25 and 40 Degrees C.

Frequency (Hz)	25°C	40°C	Ratio
0 - 50k	30.86%	24.44%	0.79
50k - 100k	26.43%	22.25%	0.84
100k - 150k	19.38%	18.45%	0.95
150k - 200k	12.17%	13.93%	1.14
200k - 250k	6.55%	9.57%	1.46
250k - 300k	3.01%	5.99%	1.99
300k - 350k	1.19%	3.41%	2.87
350k - 400k	0.40%	1.77%	4.43

According to Figure 3.21, the agreement between measurement and theory is good. But it is also noticed that the measurement ratio in the 0-50 kHz range is 1.02 and the theoretical ratio 0.79. This is due to extraneous noise in our laboratory which the sensor picks up along with the PD. The noise spectrum consists mainly of frequencies below 20 kHz so that these noises play an important role in the 0-50 kHz range. In the 50-100 kHz and the 100-150 kHz range, two ratios are almost the same, although the normalized measurement energy, because of noise is larger than the normalized theoretical energy.

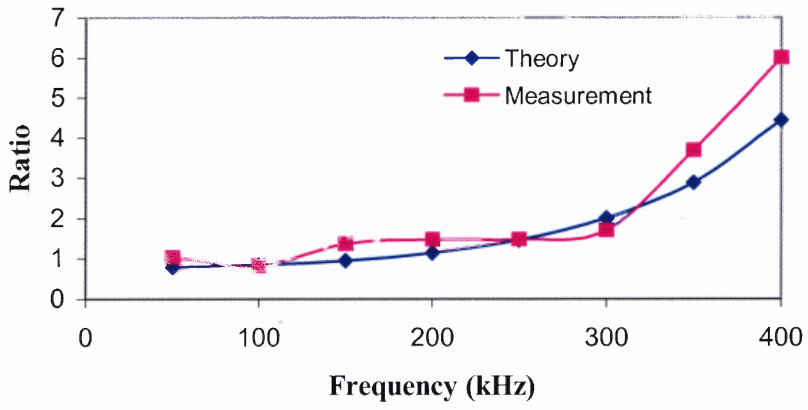

Figure 3.21 Theoretical and experimental ratios of 40 degrees C and 25 degrees C.

In the 100-400 kHz range, the experimental normalized energy is smaller than theoretical normalized energy. This is reasonable, because there is not little environment noise in this range. Considering most of environment noise in the 0-100 kHz range and noise energy also included in the total energy, the normalized energy will be smaller than normalized theoretical energy in this range.

3.5 Conclusions

A piezoelectric sensor is used for PD detection in transformer oil. For any particular medium, the spark sound signature is relatively constant from spark to spark, although the attenuation increases with distance from the source. In addition we observe that while there are 200 kHz sound wave components as expected, there are also other features, including lower frequency components. A detailed examination of spark signatures has not been reported in the literature, and deserves further investigation.

The observed persistence of the sound signature, beyond the length of the electromagnetic signal, is an important and potentially useful observation. It may be analogous to the rumble of thunder that persists significantly longer than the flash of lightning. The dominant 200 kHz frequency component within this signal appears to repeat for five or more cycles, thus it may provide an opportunity for PLL detection and the accompanying marked increase in sensitivity.

Experimental results demonstrate unequivocally the successful detection of PD spark acoustic signatures by measuring the speed of sound both in air and oil. Similar measurements using an array of sensors will enable the use of triangulation to locate the sound source. The experimental part describes the spectrum of PD at two different temperatures (25 and 40 degrees C). The detected signals are analyzed by means of FFT and their properties are discussed. Measurement of PD energy is currently a very important issue, which has attracted an interest both from academic and industrial sources. Spectral analysis of energy makes it possible to broaden knowledge of information carried by an acoustic signal. Experimental results show that acoustic energy shifting from low frequency to high frequency with increased temperature. The

theoretical analysis and simulations of PD acoustic signal energy are presented at 25 and 40 degrees C and simulation results agree with experimental results. The obtained results show the temperature of the transformer oil is one of the important factors related to PD. The impact of oil temperature changes has been evaluated on the spark signature spectrum. The measurement result is in agreement with theoretical expectation. This is possibly an important advance in spark sound diagnostics in oil.

Theoretical analysis enables us to calculate relative value of sound energy. Up-to date preferred bandwidths usually have not exceeded the frequency of 100 kHz [56] or 200 kHz [57]. It indicates the necessity to extend the measurement bandwidths with increased temperature of transformer oil.

CHAPTER 4

THE OPTIC FIBER SENSOR DEVELOPMENT

4.1 Introduction to the Optic Fiber Sensor

Optical fiber-based sensors have been shown to be attractive devices with which to measure a wide range of physical and chemical parameters because the sensors have a number of inherent advantages, including small size, light weight, high sensitivity, electrical nonconductivity, and immunity to EMI noise [58-61]. These advantages make optical fiber sensors excellent candidates for PD detection.

Fiber optical acoustic sensors have been shown useful in many applications, such as underwater hydrophones [62, 63], material property analysis, civil structure nondestructive diagnosis [64, 65], vehicle detection and traffic monitoring [66], and partial-discharge detection [67]. Early fiber optic sensors for acoustic signal detection were based mostly on fiber optic intrinsic interferometers such as all-fiber Michelson interferometers and Mach–Zehnder interferometers. Optically interrogated pressure sensors have been demonstrated in various configurations using MEMS technology [68-76]; but sensitivities of these devices are low for PD acoustic signal detection.

A diaphragm-based fiber optical Microelectromechanical System (MEMS) sensor with high sensitivity is designed and tested for on-line detection of the acoustic waves generated by PD inside high-voltage power transformers. In principle, the sensor is made according to a Fabry Perot interferometer, which is placed on a micro machined rectangular silicon membrane as a pressure sensitive element. A fiber-optic readout scheme has been used to monitor sensor membrane deflection. Sensor design, fabrication, characterization are described.

4.2 Optic Fiber Sensor System Design

The whole optical fiber sensor system is shown in Figure 4.1. The system consists of a sensor probe, a 1310-nm LED, a low noise optical receiver (photodiode) and single-mode fibers linking the sensor the optical receiver. A 1310-nm optical isolator was inserted just after the LED to reduce optical feedback to the source. The incident light is first partially reflected at the end face of the fiber. The remainder of the light propagates across the air gap to the inner surface of the diaphragm, where it is once again partially reflected. The multiple reflections travel back along the same lead-in fiber and through the same fiber coupler to the optical receiver.

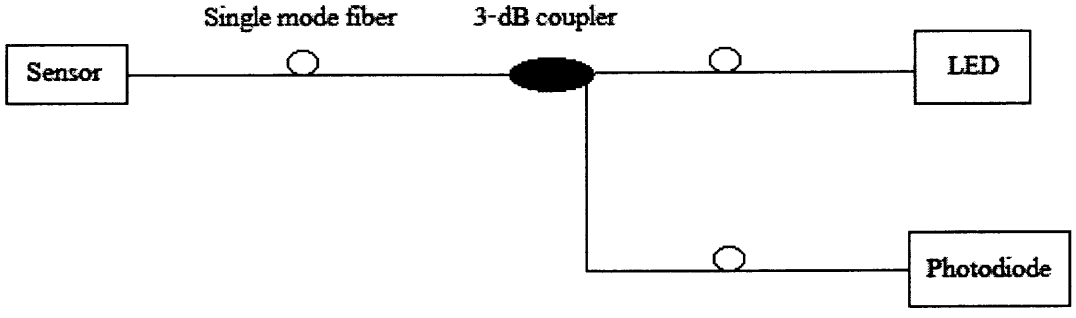

Figure 4.1 Operation principle of the fiber optical sensor.

4.3 Optic Fiber Sensor Design

The sensor described in this thesis has just one fiber. It consists of a Fabry Perot interferometer integrated into a single mode optical fiber by building dielectric mirrors into fibers. This interferometer converts the phase changes into variations of the reflected and transmitted optical power. The optical sensor is illustrated schematically in Figure 4.2.

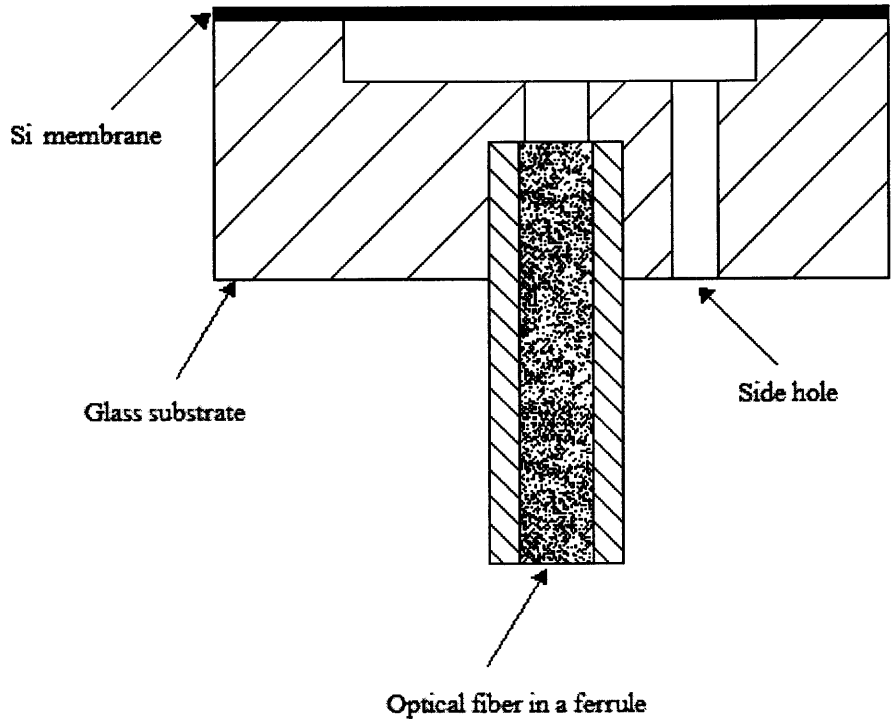

Figure 4.2 Schematic of sensor head.

The depth of square cavity is 50 μm. A center hole in glass substrate is used to place a ferruled fiber for Fabry-Perot interrogation. The cavity between the fiber end and glass surface is 105 μm wide and 40 μm deep. The width of the cavity is smaller than the fiber diameter so that the cavity serves as a stop for the fiber and sets the baseline depth of the fiber. The final chip size is about 3x3 mm. The total chip thickness is about 530 μm.

Suppose that a parallel beam of light of unit amplitude and of wavelength λ falls on a plane, parallel-sided, homogeneous, isotropic film of thickness d and refractive n_1 supported on a substrate of index n_2 as shown in Figure 4.3. The index of the first medium is n_0 and angle of incidence in this medium ϕ_0. The values of r and t for a given

boundary depend on the direction of propagation of light across the boundary. The coefficients for propagation from n_0 to n_1 are given by r_1 and t_1. The corresponding coefficients for propagation from n_1 to n_0 will be given by r_1' and t_1'.

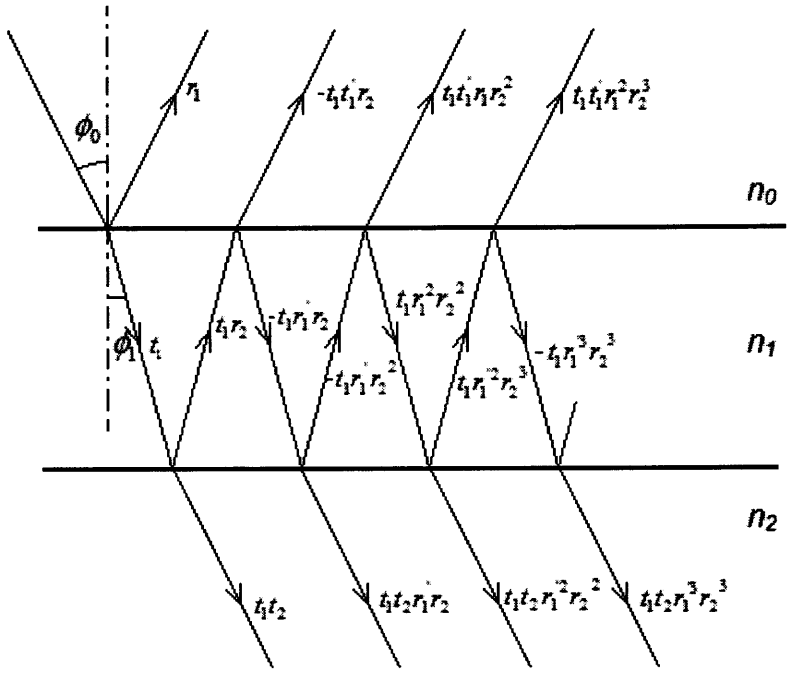

Figure 4.3 Multiple reflections of light by a single film.

The amplitudes of the successive beams reflected into medium n_0 are thus given by r_1, $t_1t_1'r_2$, $-t_1t_1'r_1r_2^2$, $t_1t_1'r_1^2r_2^3$, ... Writing θ_1, for the change in phase of the beam on traversing the film,

$$\theta_1 = \frac{2\pi}{\lambda} n_1 d \cos\phi_1 \qquad 4.1$$

The reflected amplitude is thus given by

$$R = r_1 + t_1 t_1' r_2 e^{-2i\theta_1} - t_1 t_1' r_1 r_2^{\,2} e^{-4i\theta_1} + \ldots.$$

$$R = r_1 + \frac{t_1 t_1' r_2 e^{-2i\theta_1}}{1 + r_1 r_2 e^{-2i\theta_1}} \tag{4.2}$$

$$t_1 t_1' = 1 - r_1^{\,2} \tag{4.3}$$

$$R = \frac{r_1 + r_2 e^{-2i\theta_1}}{1 + r_1 r_2 e^{-2i\theta_1}} \tag{4.4}$$

The energies of the corresponding beams are given by [77]:

$$RR^* = \frac{r_1^{\,2} + 2r_1 r_2 e^{-2i\theta_1} + r_2^{\,2}}{1 + 2r_1 r_2 e^{-2i\theta_1} + r_1^{\,2} r_2^{\,2}} \tag{4.5}$$

The reflectance (defined as ratio of reflected energy to the incident energy) is given by

$$\boldsymbol{R} = \frac{r_1^{\,2} + 2r_1 r_2 \cos 2\theta_1 + r_2^{\,2}}{1 + 2r_1 r_2 \cos 2\theta_1 + r_1^{\,2} r_2^{\,2}} \tag{4.6}$$

The output of the optical sensor can be expressed by Equation 4.6. In the sensor, the bean is in normal incidence ($\phi_0 = 0$) and media include glass, air and silicon as shown in Figure 4.4. Since $n_0 > n_1$ and $n_2 > n_1$,

$$r_1 = \frac{n_0 - n_1}{n_0 + n_1} > 0$$

$$r_2 = \frac{n_1 - n_2}{n_0 + n_1} < 0$$

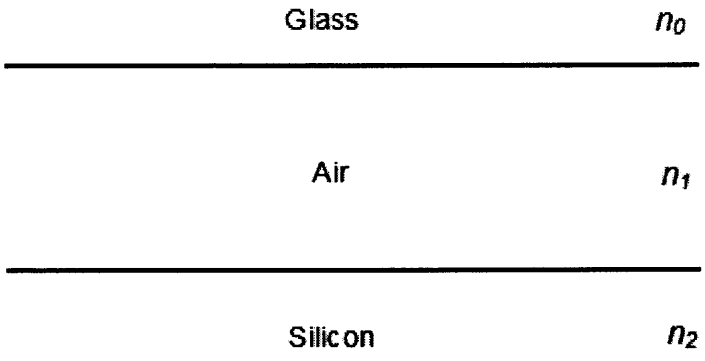

Figure 4.4 Reflection media in the fiber optic sensor.

For a fiber optic sensor, it is useful to plot the detected intensity versus gap length d, as shown in Figure 4.5. The fringe contrast drops as the gap length increase. According to the figure, one period of fringe variation corresponds to an air-gap change of one half of the optical wavelength, which in our case is 0.655 um. In principle, continuous tracking of phase changes in the interference fringes can yield information about air-gap

changes in the sensor element. The acoustic signal generated by PD causes deflection of the diaphragm and modulates the air-gap length. The sensor therefore yields outputs that correspond to the applied acoustic signals.

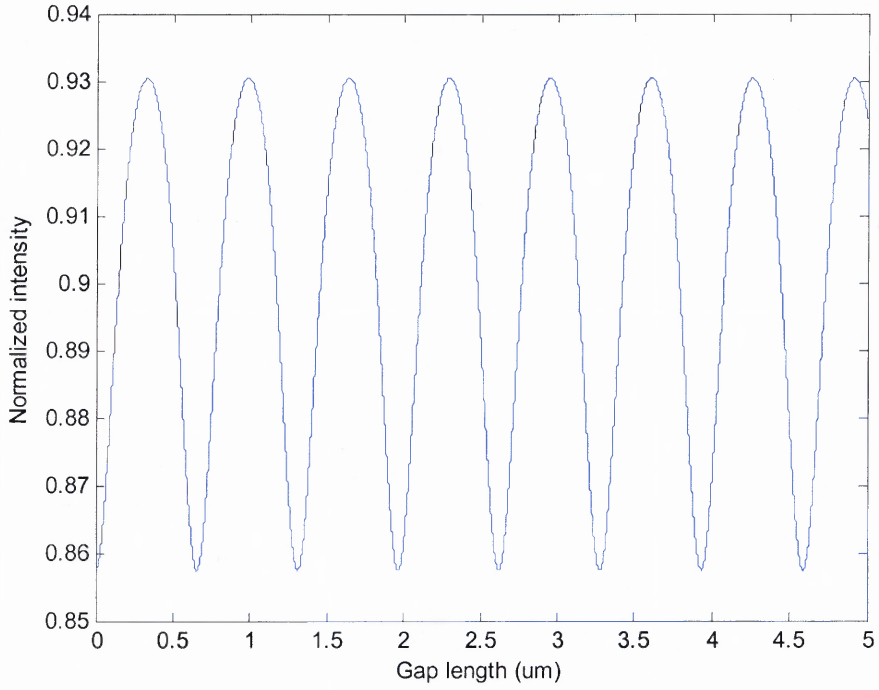

Figure 4.5 Interference fringes of the optic fiber sensor.

4.4 Optic Fiber Sensor Membrane Design

Over the last decade, silicon pressure sensors have gained in popularity. In most cases, these MEMS devices are manufactured from rectangular or circular diaphragms whose thickness is of the order of several microns [78-80]. The development of high-performance diaphragm structure is of critical importance in the successful realization of the devices. In particular, diaphragms capable of linear deflection are needed and are essential in many pressure sensors.

The load-deflection method is a well-known method for the measurement of elastic properties of thin films. In this technique, the deflection of a suspended film is measured as a function of applied pressure. The load-deflection relation of a flat square diaphragm is given by [81]:

$$\frac{Pa^4}{Eh^4} = \frac{4.2}{(1-v^2)}\left[\frac{y}{h}\right] + \frac{1.58}{(1-v)}\left[\frac{y}{h}\right]^3 \qquad 4.7$$

Where

P applied pressure (Pascal),

y the center deflection of the diaphragm

a the half side length,

E young's modulus,

h the diaphragm thickness,

v Poisson's ratio of the diaphragm material.

The deflection range is divided into two regions: a small deflection region and (deflection less than 25% of the diaphragm thickness) described by the linear term in Equation 4.7, and a large deflection region described by the non-linear, cubic term in Equation 4.7. As a general rule, the deflection of the diaphragm at the center must be no greater than the diaphragm thickness; and, for linearity in the order of 0.3%, should be limited to one quarter the diaphragm thickness.

The linear part can be expressed by

$$y = \frac{Pa^4(1-\nu^2)}{4.2Eh^3} \tag{4.8}$$

In order to increase the sensitivity, the diaphragm thickness should be thin to maximize the load-deflection responses. On the other hand, thin diaphragm under high pressure may result in large deflection and nonlinear effects that are not desirable. It is therefore important to characterize the relationship between diaphragm thickness, deflection, and sensitivity, in order to establish the design guidelines for micro pressure sensors.

For a diaphragm clamped on its edges, from a mathematical point of view, the diaphragm can be viewed as a thin plate and the exact solution for the differential equation that describes its oscillation is given in [82]. Assuming that the deflection of the diaphragm is small compared to its thickness. The Rayleigh-Ritz method [83] was used to find the frequency of the lowest mode of vibration. The relationship for the fundamental frequency for a square plate having density ρ_d and oscillating in a medium (ρ_m) is found to be:

$$f_1 = \frac{10.21}{a^2\sqrt{1+\beta}}\sqrt{\frac{gD}{\rho_d h}} \tag{4.9}$$

Where g is acceleration of gravity, β and D are given by:

$$\beta = 0.6689 \frac{\rho_m}{\rho_d} \frac{a}{h}$$

$$D = \frac{Eh^3}{12(1-\mu^2)}$$

Figure 4.6 shows the relationships among the side length, thickness, and natural frequency of the diaphragm. With a given side length, the resonant frequency increases with thickness. With a given thickness of diaphragm, the frequency decreases with side length. Figure 4.6 also shows us that thickness has more effect on resonant frequency than side length.

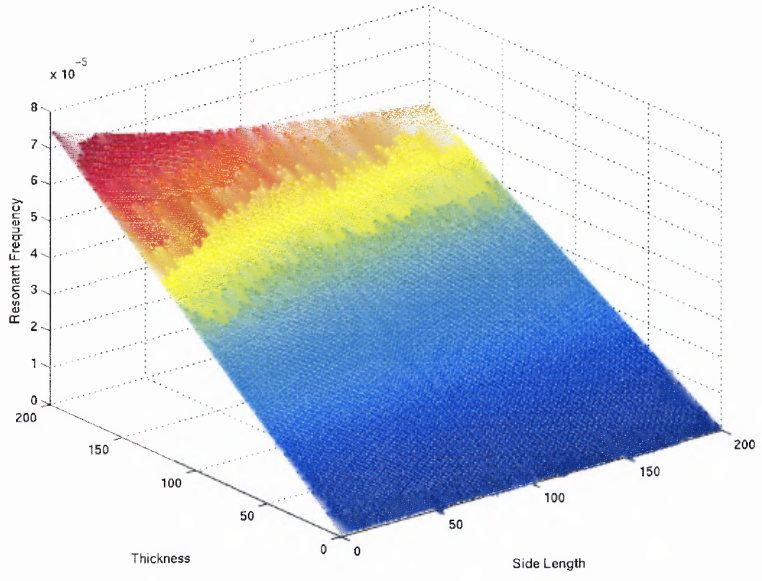

Figure 4.6 The relationships among the side length, thickness, and natural frequency with a given pressure (100 Pa).

Given E 150 GPa and v 0.25, Equation 4.8 become

$$a = \left(\frac{4.2Eh^3 y}{(1-v^2)P}\right)^{1/4} = \left(\frac{50.4Dy}{P}\right)^{1/4} \quad 4.10$$

Equation 4.9 becomes:

$$f_1 = 4.5\left(\frac{P}{y\left(\rho_d h + 0.6689\rho_m\left(\frac{y}{P}\right)^{1/4} h^{3/4}\right)}\right)^{1/2} \quad 4.11$$

Where ρ_d is 2330 kg/m^3 and ρ_m 1.25 kg/m^3.

When a pressure (100 Pa) is applied to the diaphragm, the relationships among natural frequency, deflection and thickness of diaphragm are shown in Figure 4.7. The figure shows that in order to get large natural frequency and large deflection at the given pressure, the thickness should be thin.

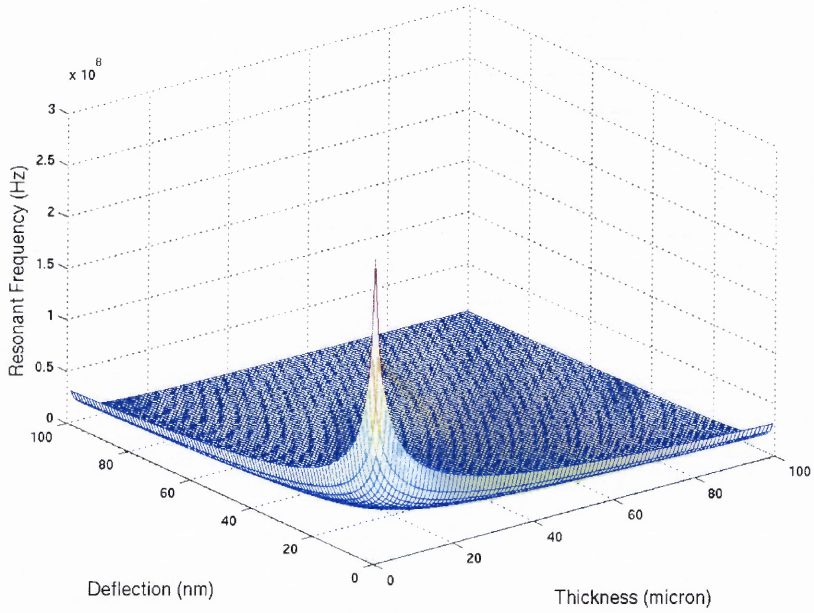

Figure 4.7 The relationships among the natural frequency, deflection and thickness of diaphragm with a given pressure (100 Pa).

According to Equation 4.8,

$$h = \left(\frac{Pa^4(1-\nu^2)}{4.2Ey} \right)^{1/3} \tag{4.12}$$

With given value of E and ν, Equation 4.11 becomes

$$f_1 = \frac{467.5P^{1/3}}{a^{2/3}y^{1/3}\left(\rho_d + 5863\rho_m \left(\frac{y}{aP} \right)^{1/3} \right)^{1/2}} \tag{4.13}$$

When a pressure (100 Pa) is applied to the diaphragm, the relationship among the natural frequency, deflection and diameter of diaphragm is shown in Figure 4.10. Figure 4.10 tells us that in order to get large natural frequency and large deflection of diaphragm at given load, the side length need to be small.

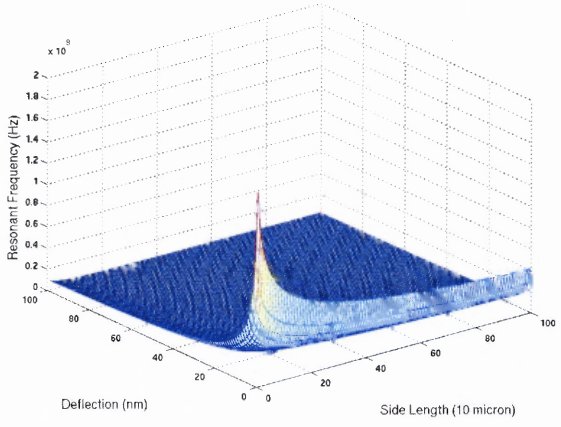

Figure 4.8 The relationship among the natural frequency, deflection and side length of diaphragm with a given pressure (100 Pa).

The thickness and side length of the sensor membrane are selected depending upon the pressure range within which the device is required to operate. Due to the high sensitivity requirement for PD acoustic detection, a silicon membrane with a thickness of 25 μm and a side length of 2 mm is selected. ANSYS simulation shows that the natural frequency of the membrane is around 91 kHz as show in Figure 4.9.

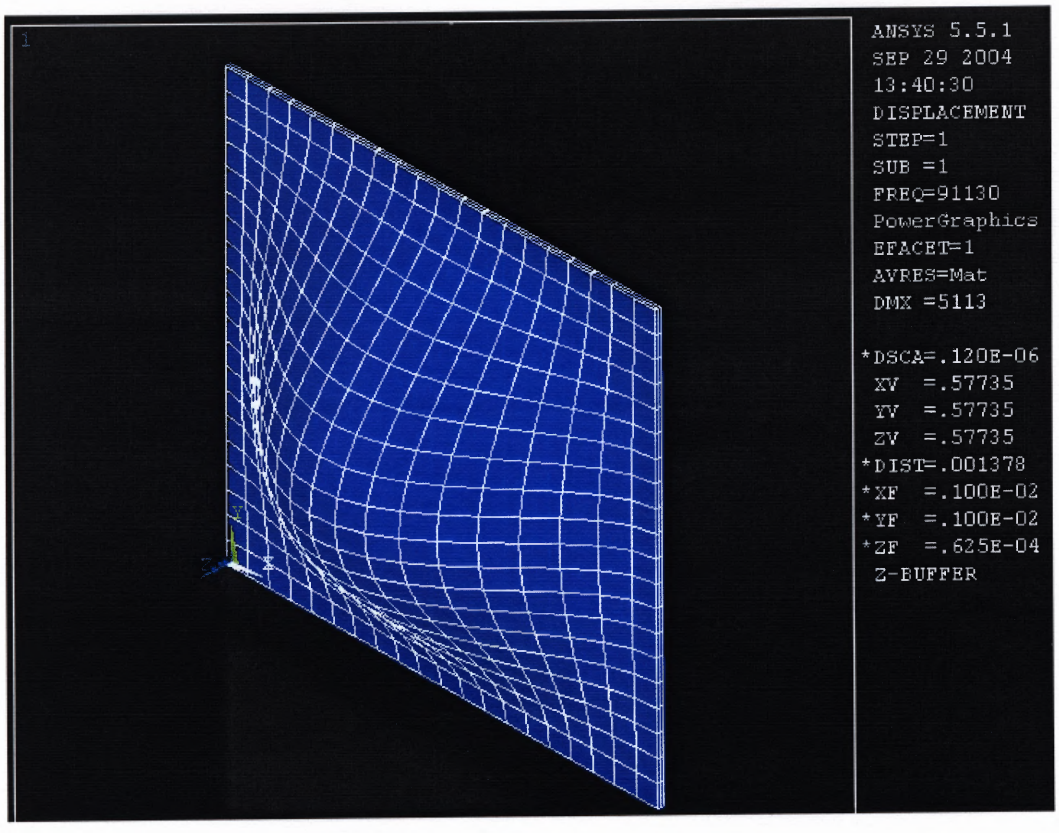

Figure 4.9 ANSYS simulation of the silicon membrane.

4.5 Optic Fiber Senor Fabrication

4.5.1 Introduction to Anodic Bonding [84-87]

A metal can be bonded to glass at relatively low temperatures using an applied voltage. The same principle can be used to bond glass to silicon. The glass is normally a sodium glass like Corning 7740. When an external electric field is applied at elevated temperature the positive ions in the glass move and create a depletion layer in the glass near the silicon surface. The voltage drop over this depletion layer creates a large electric field that pulls the wafers together. The bonding is carried out at 180-500C near the

annealing point but well below the melting point of the glass. The bonding is formed by silicon bonds to oxygen in the glass. The voltage applied is in the range 200-1000 volts.

Anodic bonding is less sensitive to small particles or roughness of the surface, careful cleaning of the wafers. The glass used in the process must be slightly conducting at the chosen bonding temperature. The bonding process can be monitored by observing the current which starts with a peak when the voltage is applied and then decreases. The bond will normally be good when the current has reached about 10-30% of its initial value. Normal bonding time is about 5-10 minutes but up to half an hour can also be needed.

4.5.2 Anodic Bonding of Silicon and Glass Wafer

During this thesis work, an automated bonding system from Electronic Vision Inc. is used. The EV501S is capable of performing direct, anodic and thermal compression bonding, under vacuum or in a supplied gas, of wafers 4, 5 and 6 inches in diameter in a repeatable fashion. As much as 2000 volts can be applied for anodic bonding, 2500 Newton pressure for thermal/compression bonding, vacuum as low as 10-6 Torr and the wafers can be individually heated up to 550°C.

If at lest one material is insulating, an applied voltage across the wafer stack may help in bonding. The mechanics are not fully known, even for silicon to glass, but the process generally involves elevated temperature (300-550°C) and high voltage (400-1000 V). Because of the elevated temperatures, material with similar thermal coefficients of expansion (TCE) should be used to avoid high interface stress, which could lead to cracking or debonding, upon cooling down.

With its closely matching TCE, Pyrex code 7740 is commonly bonded to silicon. Pyrex consists of about 80% SiO_2, 13% B_2O_3, 15% Na_2), and 2.35% Fe_2O_3, Al_2O_3. The large voltage applied creates an electrostatic field in the gap between wafers. At the elevated temperatures commonly used, sodium ions are mobile and tend to be drawn away from the interface if the silicon wafer is biased positive with respect to the glass. This results in a space charge region at the interface that promotes attraction to the silicon surface.

The bonding chemistry is understood less well. The high electrical voltage is assumed to cause oxygen ions to leave the glass and react with silicon to form an observed oxide at the interface. The assumption is strengthened by the fact that anodic bonding of silicon and Pyrex is not completely reversible. If the bias is made such that the glass is now positive with respect to the silicon, the oxide layer does not completely dissociate and the wafers remain bonded. Because of the high electric field and resulting space charge region that promotes bonding, surface roughness and flatness is less critical than for direct wafer bonding.

The pressure sensor head, consisting of the thin silicon membrane and the glass substrate (as shown in Figure 4.10) with cavity and fiber through hole, is fabricated in one clean room step: anodic bonding. After anodic bonding, the silicon wafer is bonded to glass wafer (as shown in Figure 4.11). The thickness of the thin silicon wafer is selected depending upon the pressure range within which the device is required to operate. The wafer is diced to make the optical sensor head. A difference in pressure between the exposed and internal surfaces of the membrane causes a deflection. Figure 4.12 shows the optical sensor structure and dimensions. When the sensor was inserted inside the

transformer, static oil pressure can be as high as 8 psi which will make the diaphragm work in the nonlinear region. In our sensor, an additional hole is drilled through the glass wafer into the cavity. Pressure measurements are then related to the surrounding pressure.

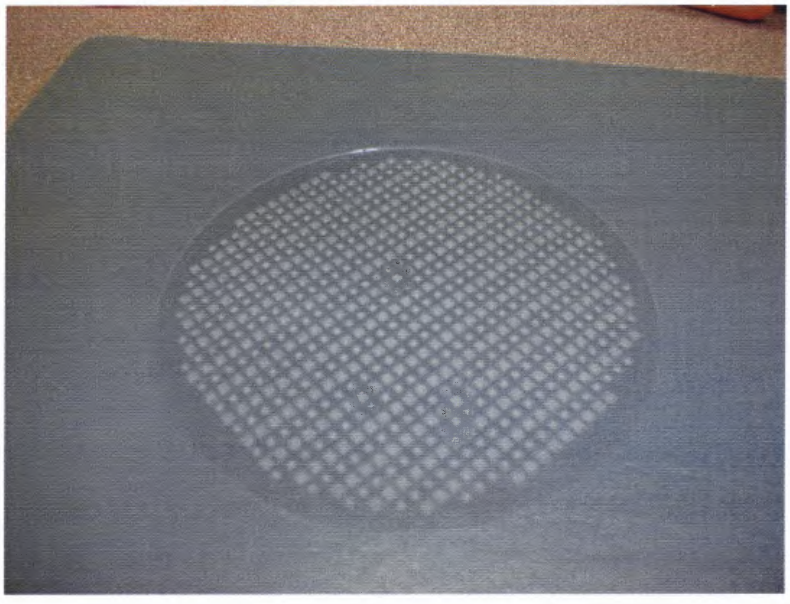

Figure 4.10 The glass wafer.

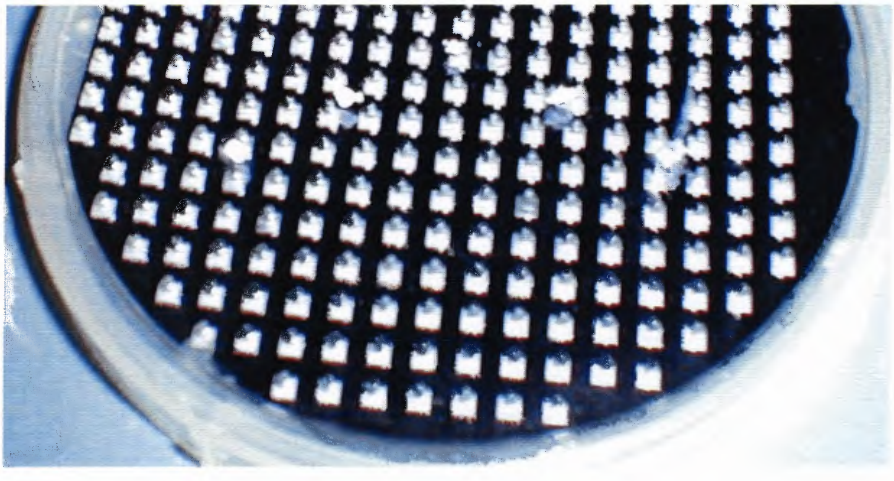

Figure 4.11 Silicon wafer bonded to glass wafer.

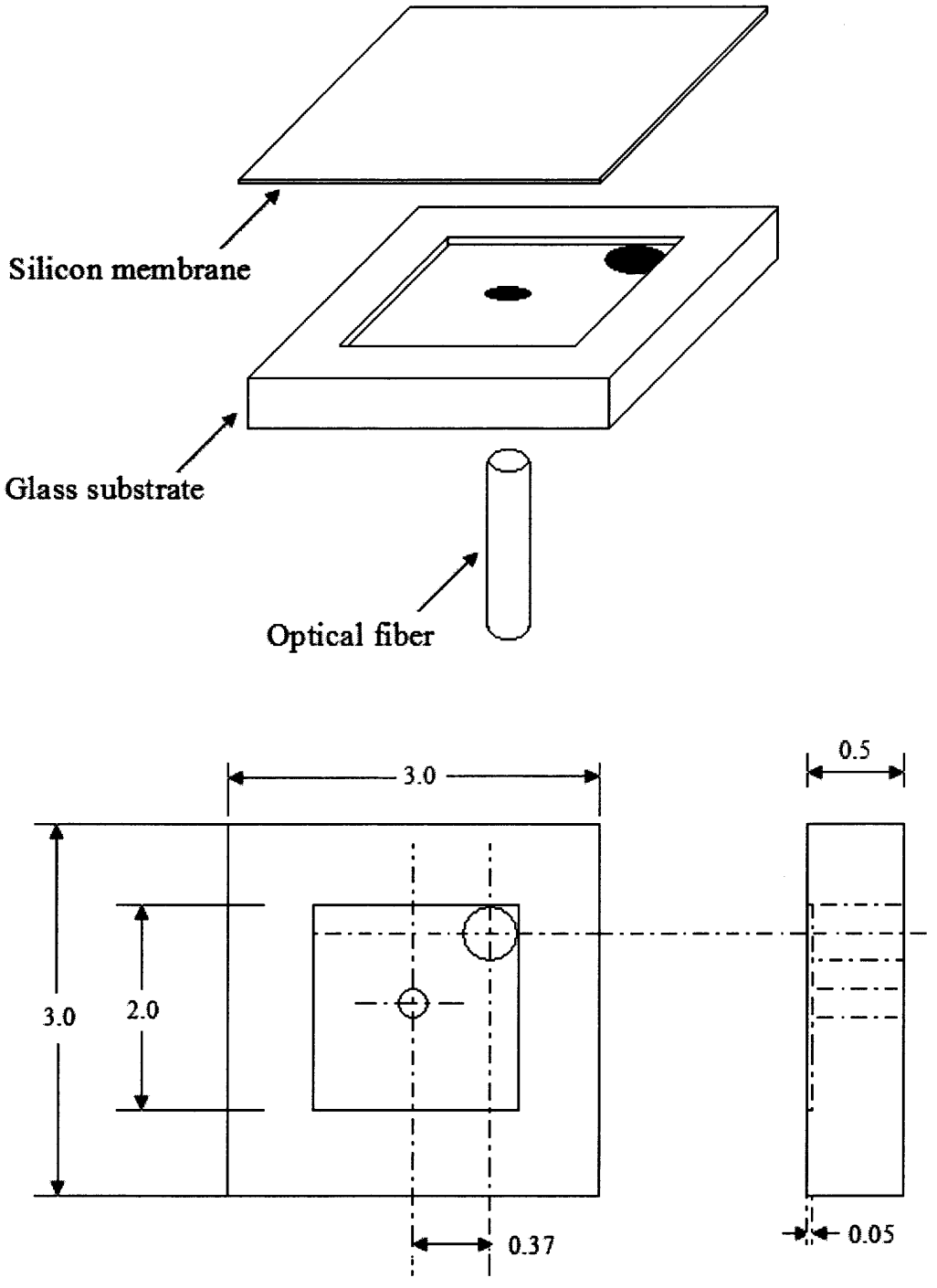

Figure 4.12 Sensor structure and dimensions.

4.5.3 Evaporation of Gold to the Silicon Wafer

Figure 4.13 shows relationship between reflectance and sensor output (Given the reflectance between fiber end and air is 3.5%, cavity length of 90 μm, and light source wavelength of 1.31 μm). The sensor output increases when the interface reflectance increases. The reflectance of the air/silicon interface at 1310 nm is about 30% at normal incidence, although higher than that of the air and glass of 4%, a layer of gold is evaporated (about 200 angstroms) to the silicon membrane to increase the reflectance.

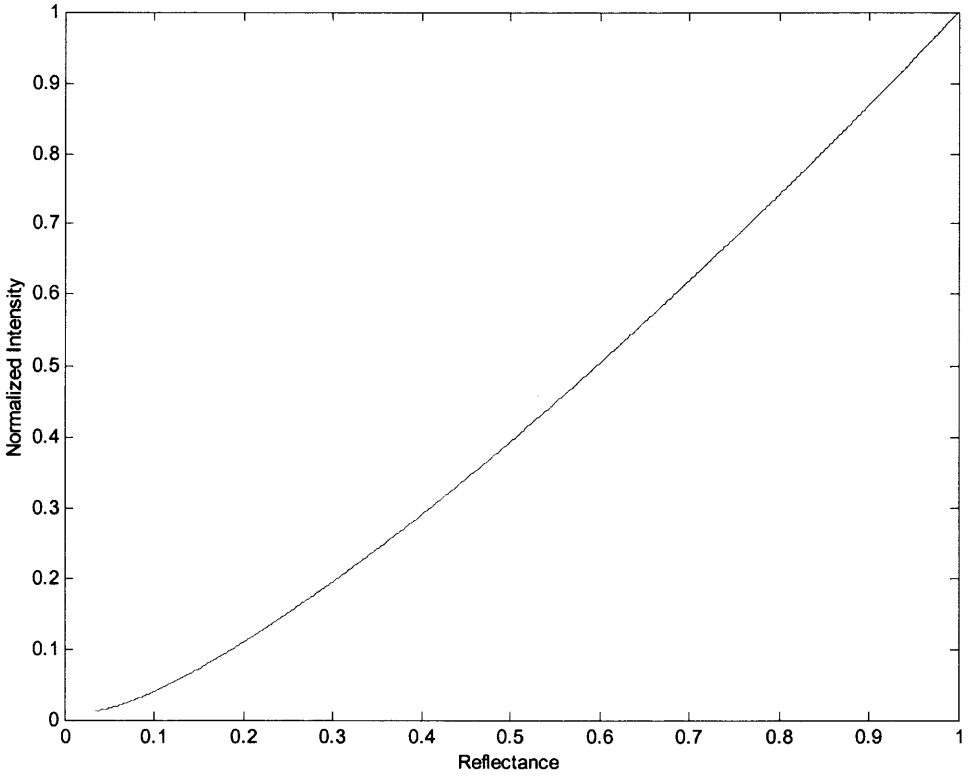

Figure 4.13 Relationship between reflectance and output intensity.

4.5.4 Sensor Packaging

A stainless steel housing for the sensor has been designed and fabricated. The housing is illustrated in the engineering drawings in Appedix A, and a finished system is shown in Figure 4.14. The sensor is placed at the end of a tube approcaimately 7 inch long that can be attached to a drain plug by a compression fitting connection. The end of the housing opposite the sensor has a stainless steel tee fitting for passing the optical fiber and allowing control of the sensor backside pressure and environment, as described above.

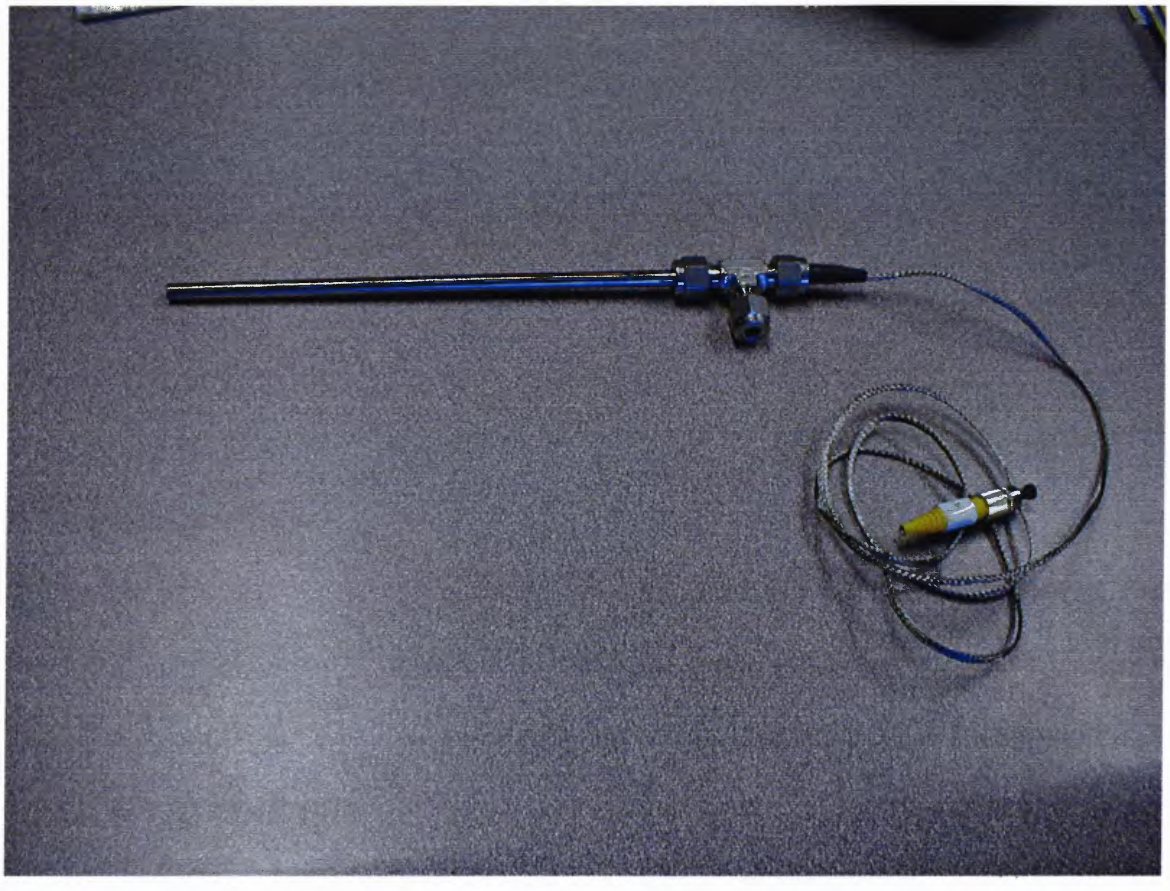

Figure 4.14 A packaged optical sensor.

4.5.5 Sensor System Development

Figure 4.15 shows the schematic of the whole optic fiber sensor system. The optoelectronic signal-processing unit consists of three main parts: light source, fiber connection (FC), and electronic pre-amplifiers. In the system, a laser light source is used as the light source. Photodiode module (model T-11-155-P-SFC) is used to convert the optical signal to the electrical signal.

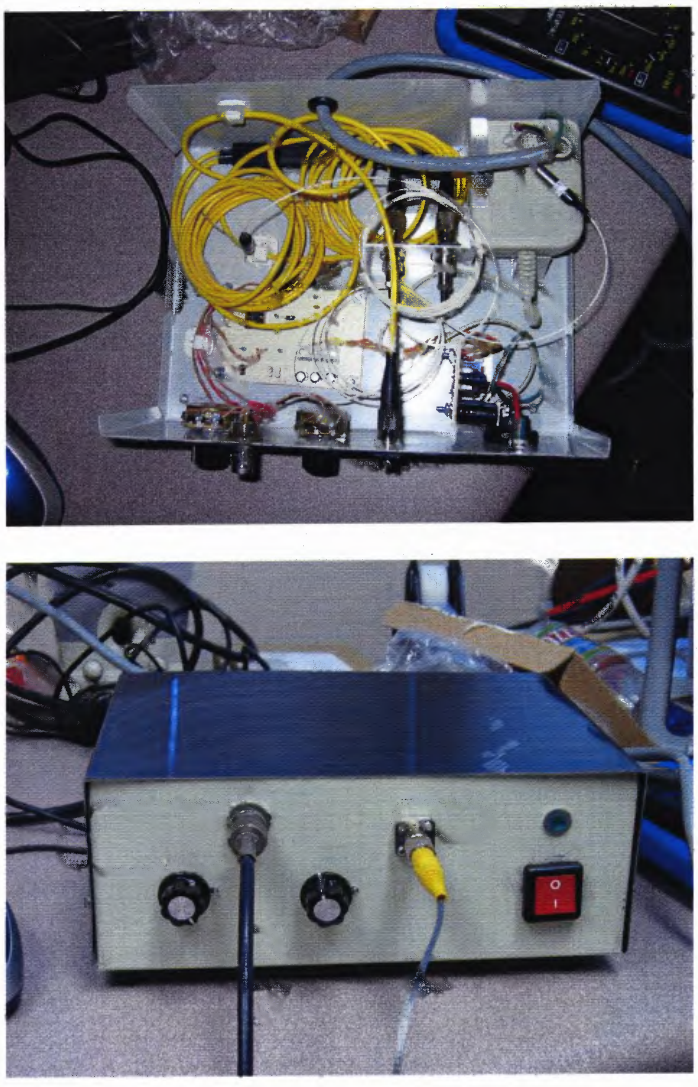

Figure 4.15 Sensor operation system.

4.6 Sensor Characterization

Characterization of the optical sensor includes three parts: sensitivity, dynamic response, and resolution.

4.6.1 Sensitivity

The sensitivity experiment setup is shown in Figure 4.16. A Motorola sensor is used as a reference sensor that is used for calibration of the applied pressure. The sensor has linear output (1 V to 5 V) when the applied pressure is from 0 to 4 kPa. Since the sensor system noise is 100 mV, the smallest pressure that the Motorola sensor can measure is 100 Pa. The fiber optical and a Motorola sensor (MPXV5004GC6U) are connected to the same pressure source using a T-connector. Tube fittings make non-leakage connections between the T-connector and the plastic pipe and super glue is used in the connection between sensors and plastic pipes. The outputs of the sensors are sent to a data logger, then to the computer for analysis.

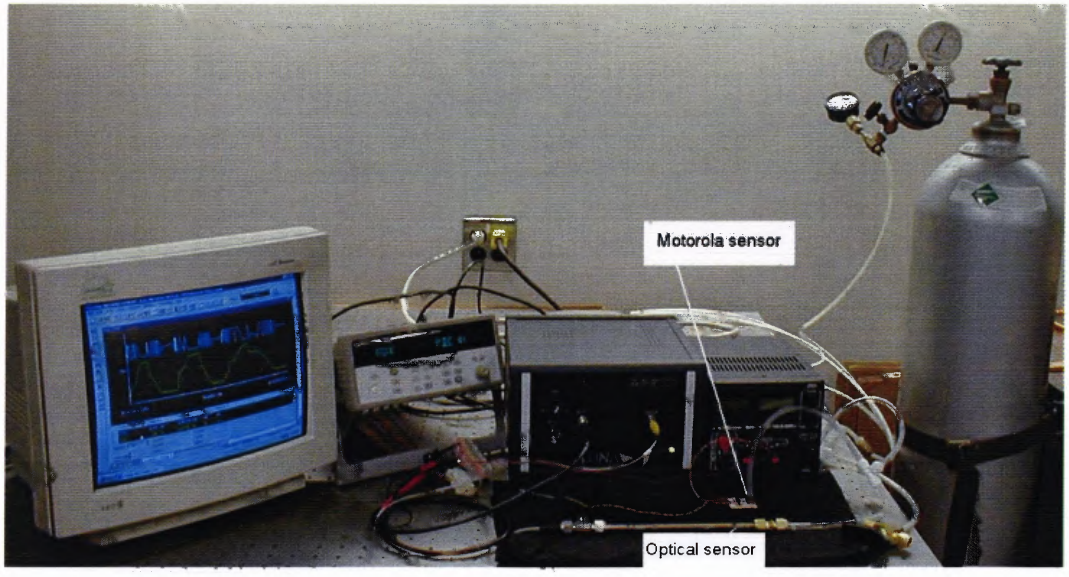

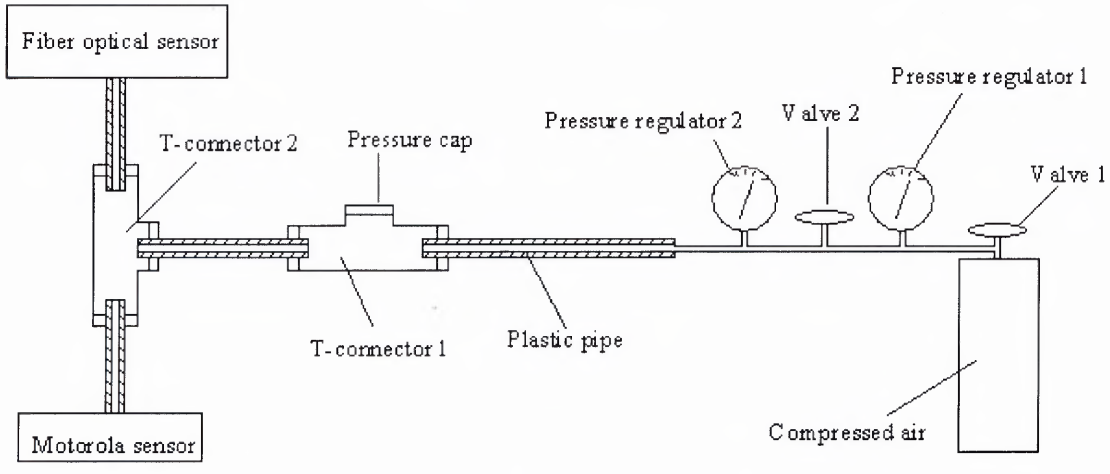

Figure 4.16 Sensitivity experimental setup.

The valve 1, initially closed is first opened slightly, and then the valve 2 is used to adjust the pressure until pressure regulator 2 reads around 0.6 psi (around 4 kPa). Also the opening of the T-connector 1 is closed so that air pressure can flow to the two sensors; moreover when the opening is opened, the air pressure will be released from T-connector 1 and the pressure will be dropped from 4 kPa to 0 kPa. Figure 4.17 shows the outputs of

two sensors when pressure drops from around 4 kPa to 0 kPa. According to the figure, when pressure drops to 0 kPa, the output of the Motorola sensor decreases from 5 V to 1 V due to linearity and the optical sensor has 7.25 periods. But the nonlinear output of optical sensor is found in the first 2 fringes. In order to accurately obtain the pressure applied in the optical sensor and avoid nonlinearity, only 2.7 fringes are chosen for calculation. When the output of the Motorola sensor changes from 1.7 V to 1 V (pressure change about 700 Pa), the optical sensor results in about 2.7 fringes (Figure 4.17). One fringe represents 259 Pa. This means the sensor will give a period of a fringe when a pressure of 259 Pa is applied to the sensor. Since the pressure change is not linear with the time (see output of the Motorola sensor), fringe ringing have different periods. And since each period of a fringe indicates that gap length has changed by half of the laser wavelength, 2.7 fringes indicates that the membrae deflection is 1.7685 μm. Considering the membrane thickness 25 μm and small deflection (deflection less than 25% of the membrane thickness), 1.7685 μm deflection of the membrane is in the linear range to the applied pressure. According to the membrane thickness (25 μm) and 259 Pa giving a period of a fringe, the sensor linear measurement range is 0-2490 Pa by calculation.

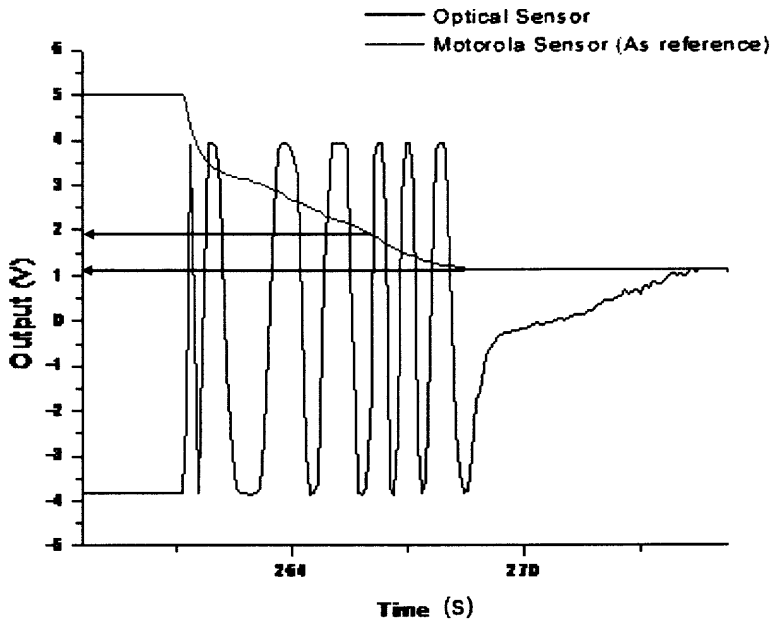

Figure 4.17 Outputs of Motorola and optical fiber sensor with the same pressure applied.

4.6.2 Frequency Response

In the experiment, a sound generator is used to produce periodic 5, 10 and 21 kHz acoustic signals which are connected to a computer speaker in air. The optical sensor is used to detect signals from the function generator and the partial discharge acoustic signals which are generated in our small tank filled with transformer oil. Then the detected signals are sent to a digital oscilloscope to demonstration and data storage.

Experimental results are shown in Figures 4.18-20. Figure 4.18 shows the optical sensor output when the function generator is producing a 5 kHz signal. Although there are some system noises along with the signals, the sensor can detect the signals of 5 kHz. Figure 4.19 shows the optical sensor output when the function generator sends a 10 kHz signal to the sensor.

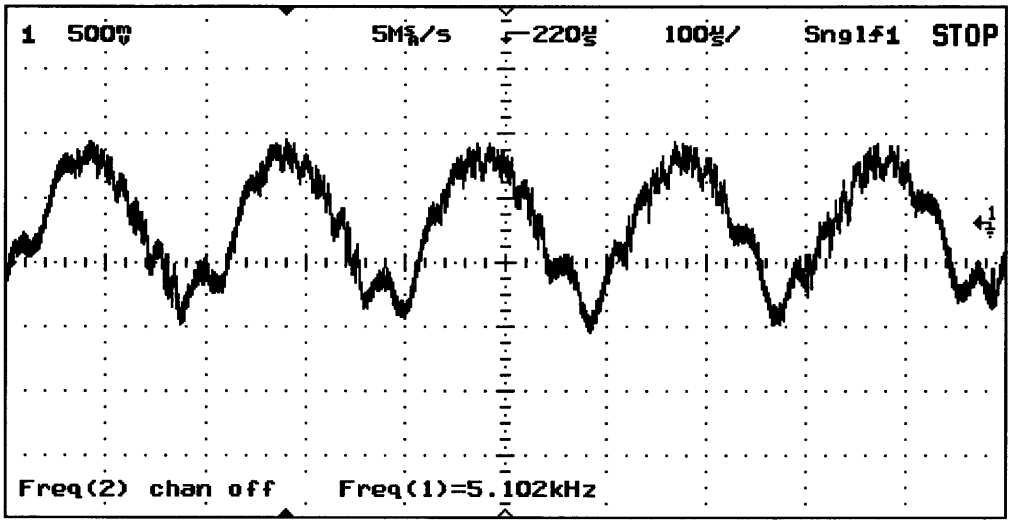

Figure 4.18 Sensor output of 5 kHz acoustic signal.

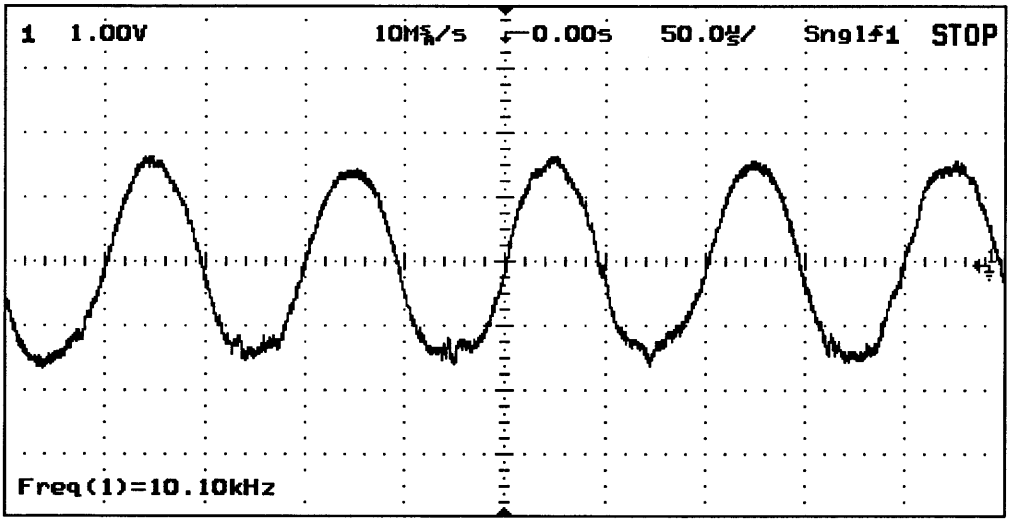

Figure 4.19 Sensor output of 10 kHz acoustic signal.

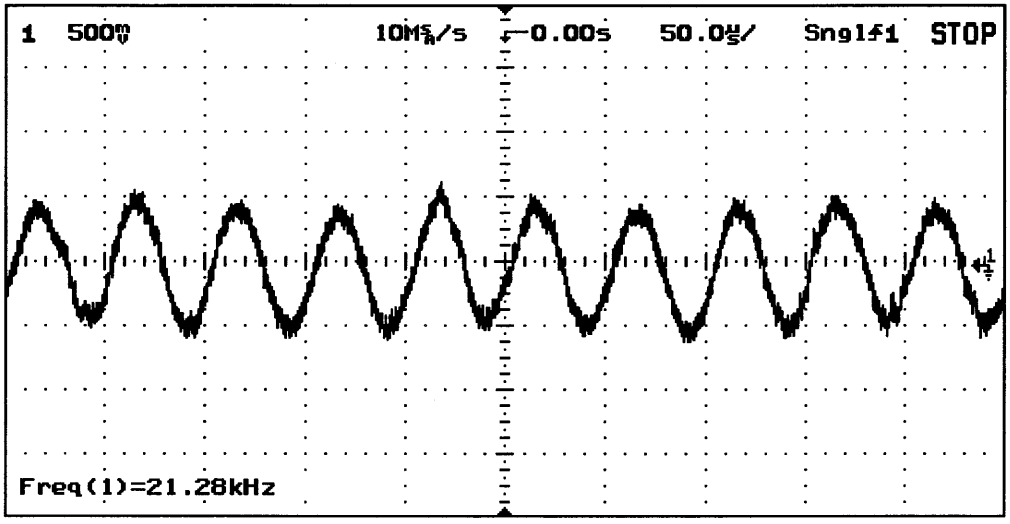

Figure 4.20 Sensor output of 21 kHz acoustic signal.

Figure 4.20 shows the optical sensor output when the function generator sends a 21 kHz signal to the sensor. According to Figure 4.18 -20, the sensor can easily detect the signals from the function generator and also show almost the same frequency as the function generator applied.

In the other experiment, the optical sensor is used to measure the acoustic signal with a single frequency (1kHz, 2kHz, up to 100 kHz) generated by a function generator. The sensor output is sent to a dynamic signal analyzer (Standford research system model SR785) for spectrum measurements. For these measurements, the dynamic siganl analyzer (the input impendence of 1 MΩ) is used to select the desired frequency to make the required spectrum (power versus frequency). The resulting measurement scans show received power in the desired frequency, and in decibels relative to one mW (dBm). Figure 4.21 shows the experiment setup for measuring the frequency response of the optical fiber sensor. The optical fiber sensor is close to a speaker and the speaker is

connected to the frequency generator which supplies the acoustic source. The output of the sensor was sent to a spectrum analyzer for analysis.

Figure 4.22 shows the sensor response to acoustic signals keeping the same amplitude and increasing the frequency to 100 kHz. For this measurement, the membrane of the optical sensor has a resonant frequency of about 90 kHz. The frequency response indicates a fairly broad resonance of about 90 kHz, with small structure peaks below this frequency. It shows that the sensor has a dynamic reposnse that is close to the expected value.

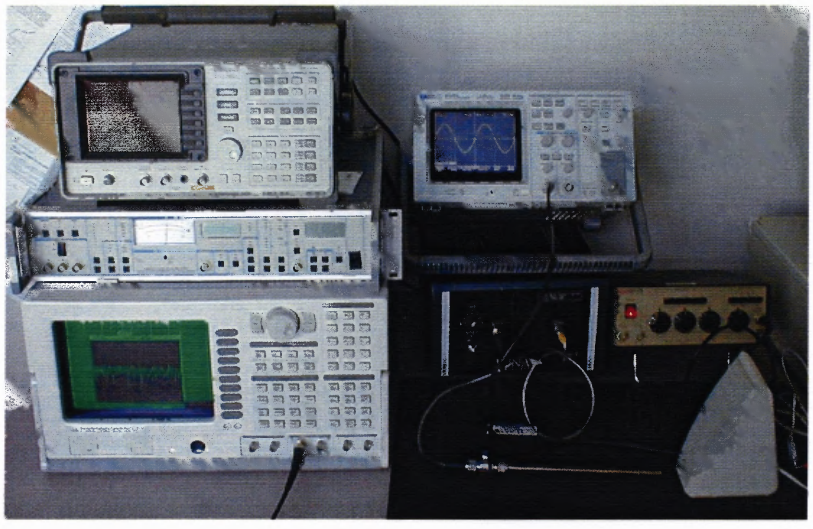

Figure 4.21 Sensor frequency response experiment setup.

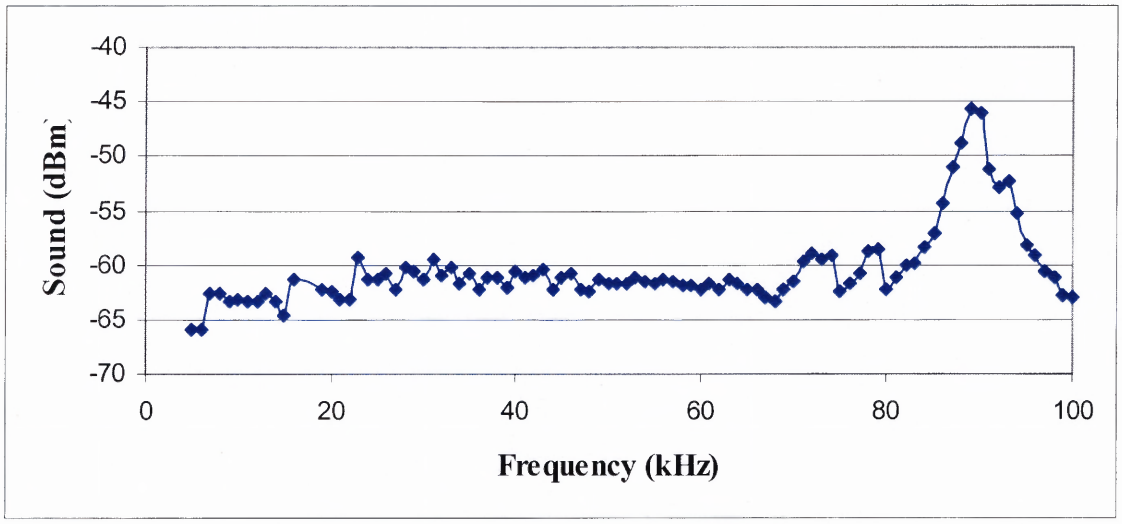

Figure 4.22 Frequency Response of the optical fiber sensor.

4.6.3 Resolution

The smallest pressure change a sensor can measure is determined by the signal-to-noise ratio of the sensor. According to Figure 4.23, the output of the optical fiber sensor noise is around 100 mV. The full output of the sensor is from -5 V to 5 V. Since 1 fringe in the optical fiber output represents 259 Pa, the smallest pressure of the sensor that can be resolved will be 1.6 Pa.

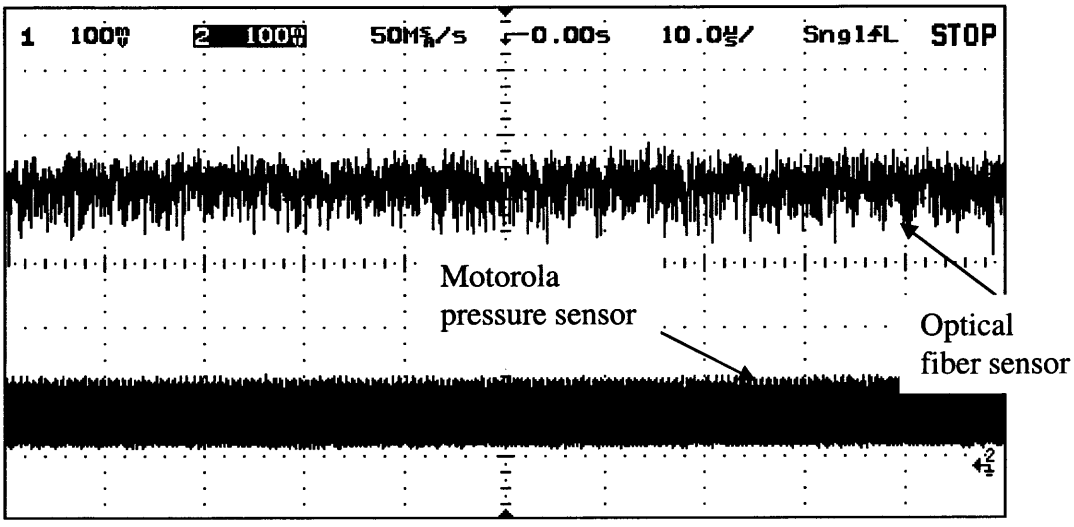

Figure 4.23 System noise of the optic fiber sensor and Motorola sensor.

4.7 Conclusions

The optical fiber sensor has been designed based on the Fabry Perot principle. The development of a high-performance diaphragm structure is of critical importance in the successful realization of the optical sensor. The relationships among silicon membrane thickness, resonant frequency and side length are investigated and simulated. According to the investigation, the silicon membrane was constructed with a thickness of 25 μm, a side length of 2 mm and a resonant frequency of about 90 kHz.

A simple micromachining process (anodic bonding) compatible with MEMS has been developed for fabricating the optical fiber sensor. Evaporation of gold to the silicon surface of the sensor was done to increase the reflectance of the air/silicon interface. An optoelectronic signal-processing unit has been designed and fabricated so as to be compatible with the signals detected by the optic fiber sensor.

The optical sensor frequency, sensitivity, and resolution have been characterized. The characterizations show that the sensor has a dynamic response that is close to the expected value of 90 kHz, also sensitivity tests shows that about 259 Pa applied pressure will give a membrane deflection of 655 nm and the pressure measurement resolution of the optical sensor is determined to be about 1.6 Pa.

CHAPTER 5

THE OPTIC FIBER SENSOR APPLICATION IN PD DETECTION

5.1 Introduction

PD occurring under oil produces a pressure wave that is transmitted throughout the transformer via the oil medium [88]. One can achieve acoustic PD detection by mounting piezoelectric acoustic sensors externally on the walls of a power transformer. An externally mounted piezoelectric acoustic sensor offers the advantages of easy installation and replacement. However, a piezoelectric sensor may suffer from degeneration of the signal-to-noise ratio caused by environmental noises such as EMI. Another disadvantage associated with an externally mounted piezoelectric sensor is that the multiple paths of the acoustic wave transmission make locating the exact positions of PD difficult. It is thus desirable to have sensors that can function reliably inside a transformer to detect clean PD-induced acoustic signals. For the sake of safety and easy installation these sensors have to be chemically inert, electrically nonconducting, passive, and small in size making optical fiber sensors excellent candidates for PD acoustic detection [89, 90]. This chapter describes the ultra sensitive optical sensor application in PD detection.

5.2 Comparisons of Piezoelectric and Optic Fiber Sensors in PD Detection

An experimental system is designed to evaluate the optical sensor performance in PD acoustic detection. The standard acoustic methods used to detect partial discharge employ piezoelectric sensors externally. As shown in Figure 5.1, the fiber optical sensor is installed in transformer oil at one end of the tank, facing a piezoelectric acoustic sensor

(Harisonic G-0504 type) at the other end of the tank. The piezoelectric sensor has an acoustic frequency response up to 5 MHz. The PD generation system (also called the PD source) is inside the tank. This arrangement is chosen because it represents many practical PD test situations in which piezoelectric sensors are attached to the sidewall of a transformer whereas fiber optical sensors can be inserted into the transformer tank. A two channel digital oscilloscope (HP Model 54616C) is used to display and store the acoustic signals detected by the two sensors.

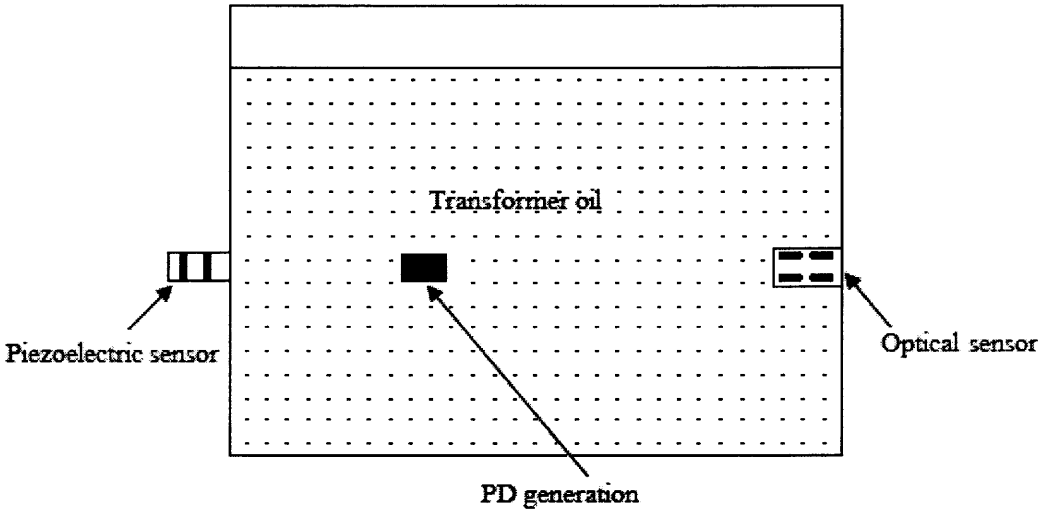

Figure 5.1 Experimental setup for PD signal detection.

The experimental results for the two sensors are shown in Figure 5.2 when they are placed at the same distance (0.4 m) from the PD source. The piezoelectric sensor almost shows no response to the acoustic signals even though the output unit has a sensitivity of 50 mV full scale, as compared to the full scale of sensitivity of 1 V for the optical sensor.

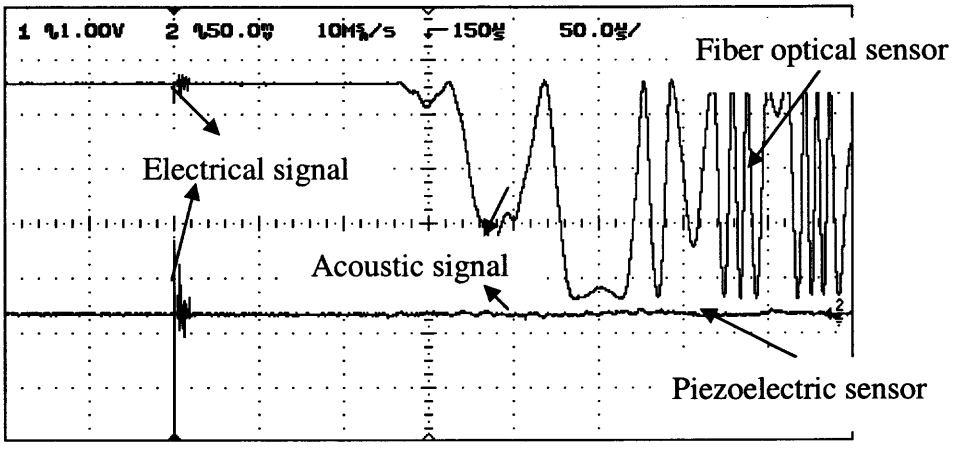

Figure 5.2 PD detection at same distance between discharge source and sensors.

Figure 5.2 shows that the electrical signal which initiates the acoustic signal is picked up by the optical and piezoelectric sensors as unwanted noise almost instantaneously in the experiment. In addition, the sensors each picks up the desired acoustic signal at the same time, although later than the electrical signal. Because of its steel housing, the optical sensor cannot be completely unaffected by the electrical signal. This prototype model using the steel housing can always be changed to some material that has no influence on electrical signals.

Since the piezoelectric sensor can't detect the signals when it is 0.4 m from the PD source, the piezoelectric sensor is mounted inside the tank and much closer to the source while the optical fiber sensor is still 0.4 m from the source. The measurement results are shown in Figure 5.3 (output voltage unit for the optical sensor is 2 v and for the piezoelectric sensor 5 mv). Due to the piezoelectric sensor being much closer to the PD source than the optical sensor, and the constant sound velocity in the transformer oil (around 1440 m/s), the acoustic signal arrives at the piezoelectric sensor earlier than the optical sensor. But the detected signal is still very weak compared to the optical sensor.

These experiments further illustrate the enhanced sensitivity and superior performance of the optical sensor when compared to the piezoelectric for PD detection.

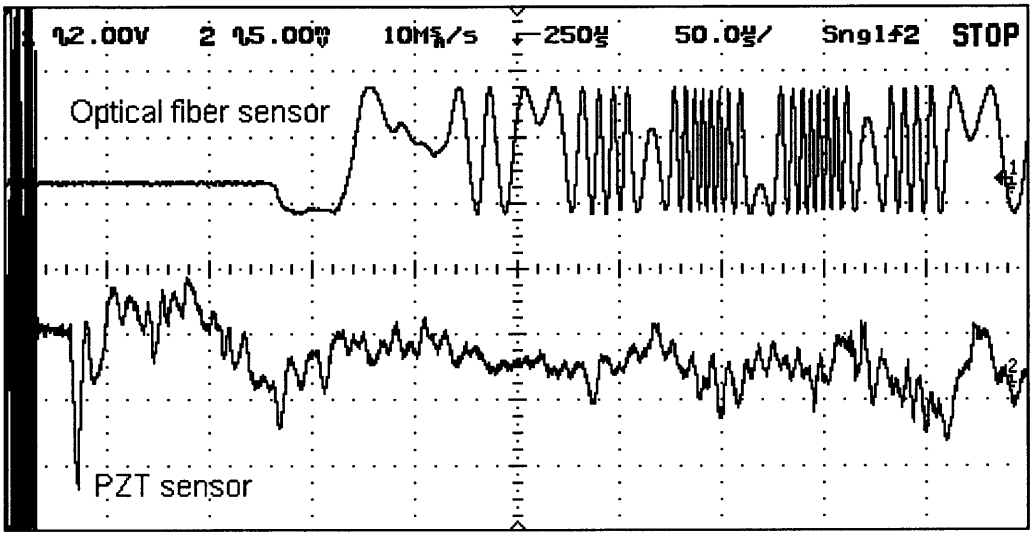

Figure 5.3 PD detection using piezoelectric and fiber optical sensors.

5.3 The Optic Fiber Sensor Detection of PD Signal and Surrounding Noises

When the optical sensor works in a real transformer, the sensor should be capable of detecting not only PD signal but also of discriminating the PD signals from surrounding noise. An experiment is designed to test the sensor's capability to pick up the PD signal from surrounding noises.

A function generator is used to generate 5 kHz signals which are sent to a computer speaker and the PD acoustic signal is generated by our PD generation unit. The optical fiber sensor receives both the 5 kHz signal and the PD acoustic signal which are then sent to the digital oscilloscope for demonstration and data storage. The experimental result is shown in Figure 5.4. According to the figure, when the sensor is faced with two different acoustic sources, the sensor clearly discriminates the different sources.

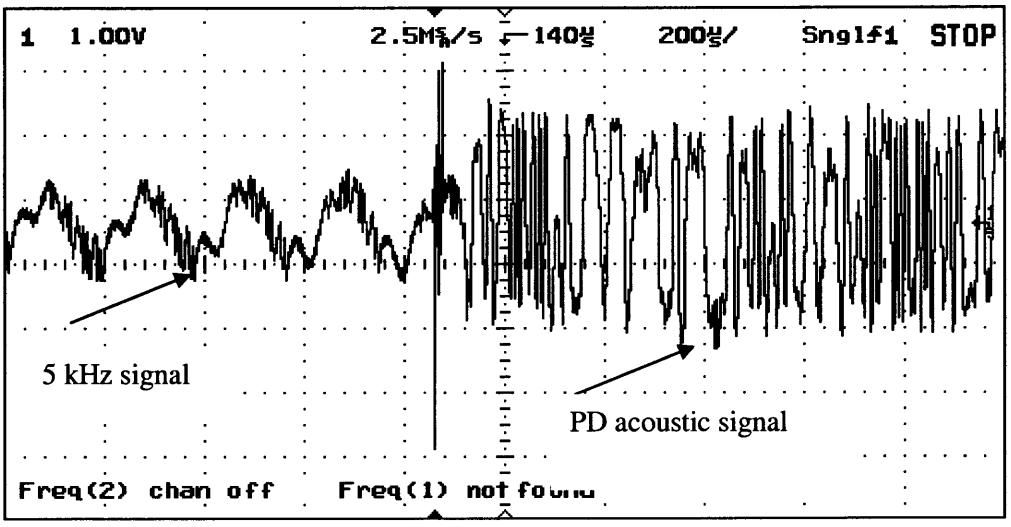

Figure 5.4 The sensor output of the PD and the 5 kHz signals from the function generator.

5.4 Optic Fiber Sensor Application in PD Localization

PDs are pulse-like in nature and cause mechanical stress waves (acoustic emission) to propagate within the transformer. These stress waves propagate throughout the surrounding oil and can be detected inside the transformer. By measuring the relative time of arrival of the acoustic wave at different locations inside the transformer, the three dimensional location of the PD within the transformer can be determined.

5.4.1 Localization Theory

Figure 5.5 shows that the acoustic wave emitted at any given point $P(x, y, z)$ in the transformer is measured by four sensors. It is assumed that the optical sensor is unaffected by the electrical signal. Then only these four sensors are needed to locate the PD position using the time-arrive-model. Each of the sensors are at known spatial coordinate S_m (X_{lm}, Y_{lm}, Z_{lm}) where l=1, 2, 3 and m=1, 2, 3, 4. The distance from the

localized PD to the sensors is given by L_n, where n=1, 2, 3, 4. As shown in the figure, the four sensors are placed in different positions to pick up sound from a PD occurring in the transformer.

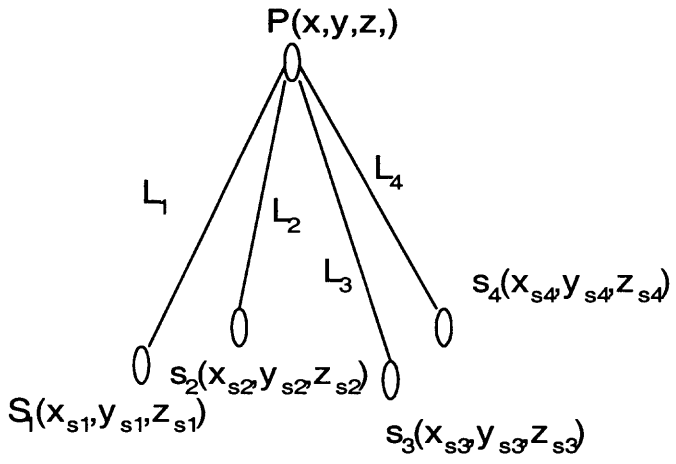

Figure 5.5 Sensor localization illustrations

Assuming the propagation time from the PD source to the acoustic sensor S_1 is T, the distance from the PD site to the four sensors is then given by the following formulas:

$$L_1 = v_0 T_1 = v_0 T \tag{5.1}$$

$$L_2 = v_0 T_2 = v_0 (T + t_{12}) \tag{5.2}$$

$$L_3 = v_0 T_3 = v_0 (T + t_{13}) \tag{5.3}$$

$$L_4 = v_0 T_4 = v_0 (T + t_{14}) \tag{5.4}$$

Where T_n (n is an integer) is the propagation time from the PD site to the sensor S_n, t_{1n} is the time delay between the sensor S_1 and S_n and v_0 is the acoustic wave propagation velocity in the oil. Therefore, the relationship between the PD position and sensors is as follows:

$$(x-x_{s1})^2+(y-y_{s1})^2+(z-z_{s1})^2=(v_0T)^2 \tag{5.5}$$

$$(x-x_{s2})^2+(y-y_{s2})^2+(z-z_{s2})^2=[v_0(T+t_{12})]^2 \tag{5.6}$$

$$(x-x_{s3})^2+(y-y_{s3})^2+(z-z_{s3})^2=[v_0(T+t_{13})]^2 \tag{5.7}$$

$$(x-x_{s4})^2+(y-y_{s4})^2+(z-z_{s4})^2=[v_0(T+t_{14})]^2 \tag{5.8}$$

Since v_0 is a constant and t_{1n} can be known by the sensor outputs, it is easy to determine the coordinates of the PD location (x, y, z).

$$x=\frac{1}{N}\sum_{i=1}^{N}x_{si}+\frac{1}{N}\sum_{i=1}^{N}\frac{(T+t_{1i})(x-x_{si})v_0}{[(x-x_{si})^2+(y-y_{si})^2+(z-z_{si})^2]^{1/2}} \tag{5.9}$$

$$y=\frac{1}{N}\sum_{i=1}^{N}y_{si}+\frac{1}{N}\sum_{i=1}^{N}\frac{(T+t_{1i})(y-y_{si})v_0}{[(x-x_{si})^2+(y-y_{si})^2+(z-z_{si})^2]^{1/2}} \tag{5.10}$$

$$z = \frac{1}{N}\sum_{i=1}^{N} z_{si} + \frac{1}{N}\sum_{i=1}^{N} \frac{(T + t_{1i})(z - z_{si})v_0}{[(x - x_{si})^2 + (y - y_{si})^2 + (z - z_{si})^2]^{1/2}} \quad 5.11$$

$$T = \frac{\sum_{i=1}^{N} [(x - x_{si})^2 + (y - y_{si})^2 + (z - z_{si})^2]^{1/2}}{v_0} \quad 5.12$$

Since every possible position of PD has a relative t_{1n}, a PD location can be calculated in advance so as to form a position table. Therefore, when data is obtained for the time delay t_{1n}, software can determine its position by comparing data stored in the table, which can speed up the location process and minimize errors.

5.4.2 2-D Localization

Localization of a PD source is always the main purpose for PD detection. The measurement setup is shown in Figure 5.6. Two optical sensors are placed in the tank at different distances from the PD source. The distance difference (L_2-L_1) between the sensors and the source is about 6 cm. The acoustic signals measured by the sensor are shown in Figure 5.7 and 5.8. The time for the acoustic signal to travel from the PD source to the optical sensors is about 60 micro second (sensor 1) and about 100 micro second (sensor 2). Since the distance between the sensors and the source is about 6 cm and measured velocity of the signal is about 1500 m/s (6cm/40micronseond). The result agrees with the previous result (acoustic velocity is 1440 m/s in transformer oil). These results show that the optical sensor can measure the speed of the PD acoustic signal accurately.

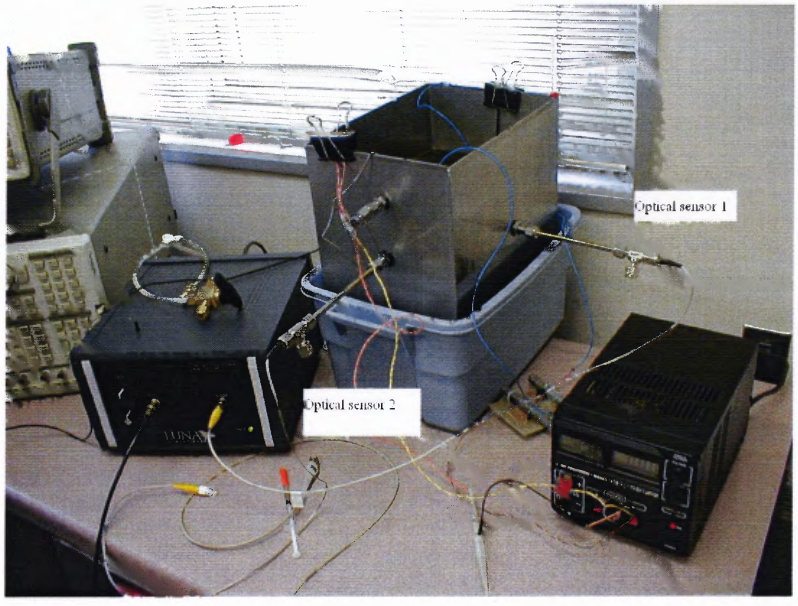

Figure 5.6 Two dimensional localization of PD experiment setup.

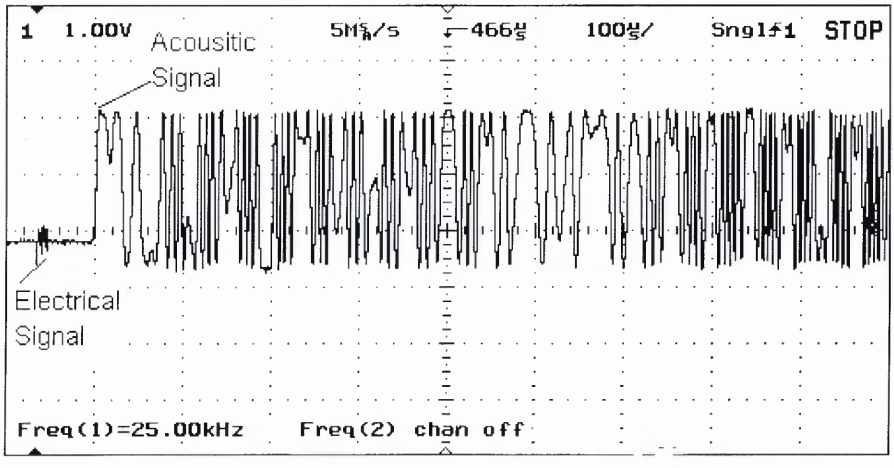

Figure 5.7 The signal response of optical sensor 1.

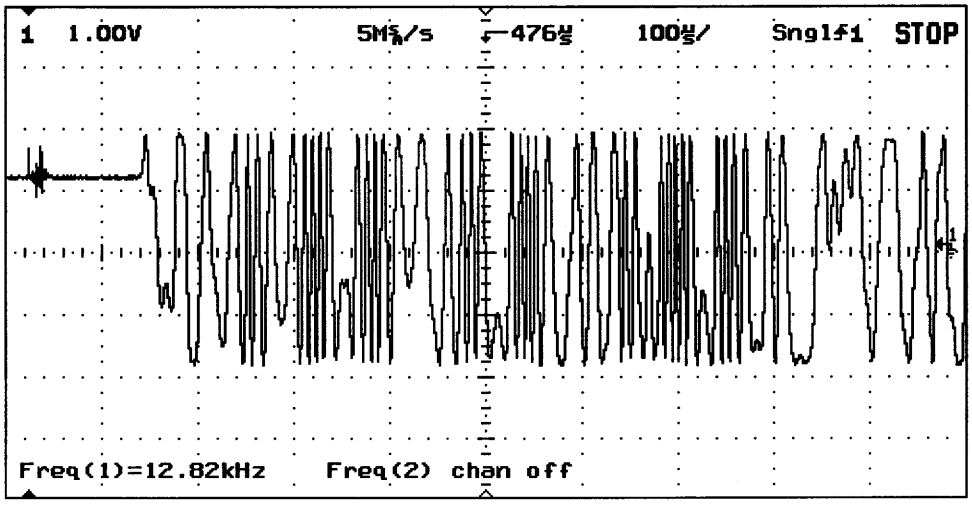

Figure 5.8 The signal response of optical sensor 2.

Since the time difference between electrical noises which is the onset of PD and the acoustic signal can be measured, the distance between the sensor and the discharge source can be calculated which is necessary to localize the PD source.

There always are some similar signals in the measurements. An experiment is arranged and designed to determine if the signals are echoes. Figure 5.9 shows the experimental setup. Initial experimental result is shown in Figure 5.10. The figure also shows that the time difference between acoustic signal and its echo is about 750 micro second. When the PD source was moved 15 cm closer to the optical fiber sensor, the measured signal is shown in Figure 5.11. The figure shows that the time difference between acoustic signal and its echo is about 1600 micro second.

By moving the PD source closer to the optical fiber sensor, the traveled distance difference between the echo and signal changed 30 cm. The time difference between the echo and signal changed by about 850 micro second. The speed of the acoustic signal is 352.9 m/s (30cm/850 micro second) which is the sound speed in air. This means that the

similar signal is indeed an echo. The echo is generated by the wall's reflection of the original acoustic signal. Details of this effect are illustrated in Figure 5.12.

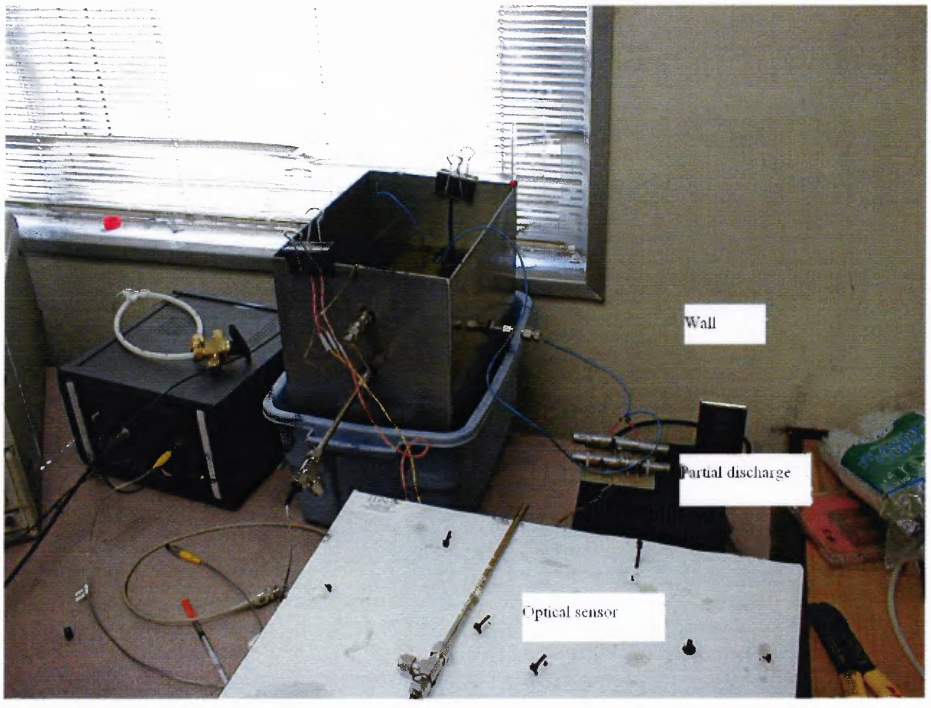

Figure 5.9 Echo experiment setup.

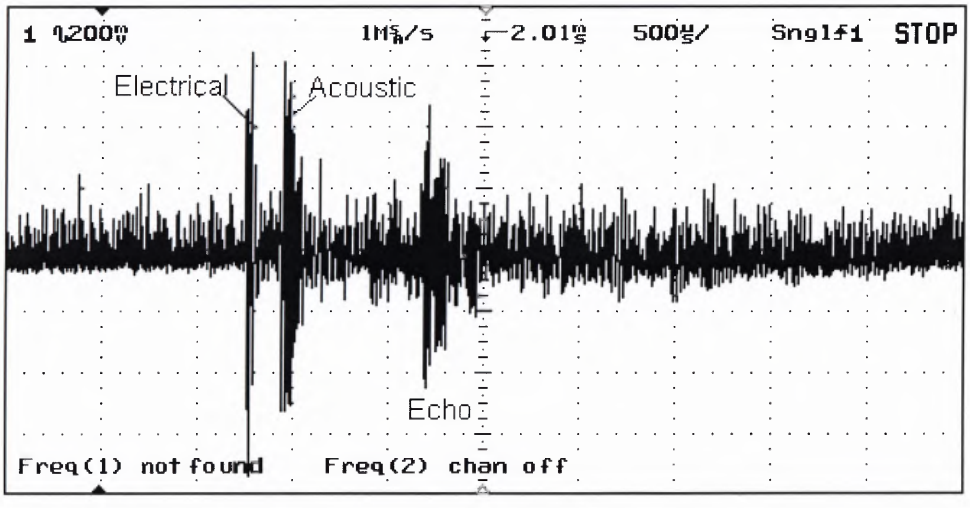

Figure 5.10 Sensor output at initial position.

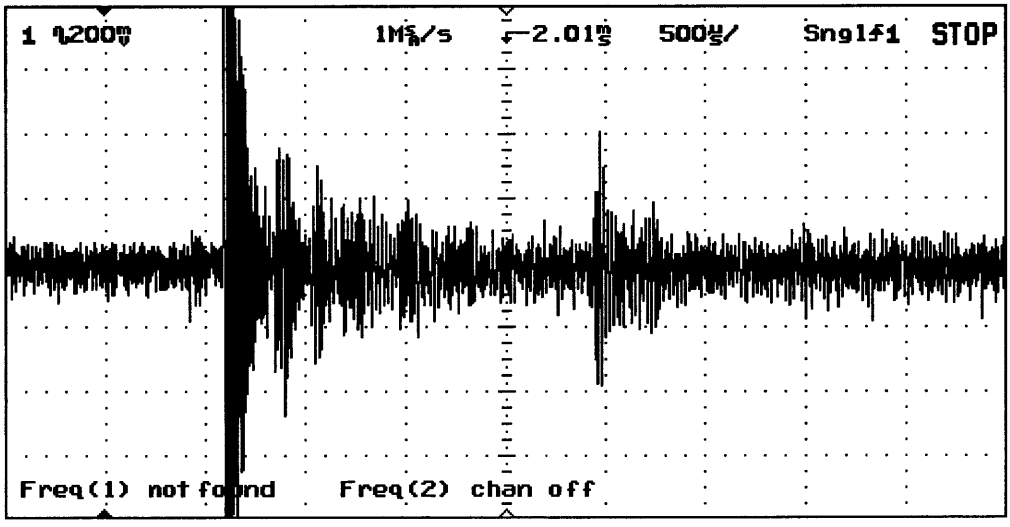

Figure 5.11 Sensor output after position changed.

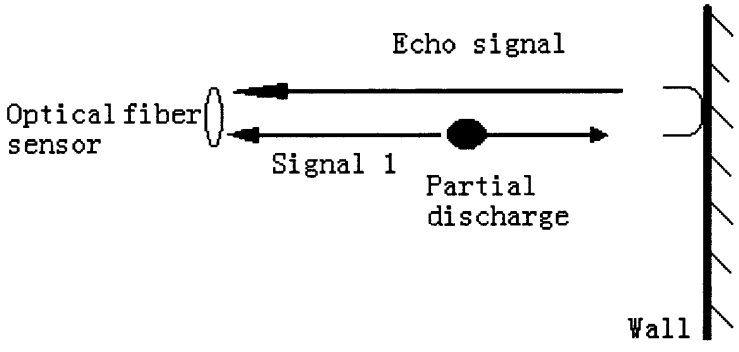

Figure 5.12 Detailed explanation of experiment design.

5.4.3 3-D Localization with Sensors Close to the Transformer Wall

The oil-filled transformer used for this experiment is shown in Figure 5.13. The transformer has a diameter of 80 cm and height of 1.2 m. Detail explanation of experimental setup is shown in Figure 5.14. Since the sensor can supply information of PD electrical and acoustic signals, only three sensors are needed for PD localization. The optical sensors are in three positions at the same height level of 5 cm below the

transformer oil surface. This setup makes sure that there is the same static pressure applied in all of the sensors, each of which is contacting the transformer wall. The PD source is in the bottom of the transformer. The detected signals at three different positions are shown in Figure 5.15 (1-3). According to the time difference (between the electrical signal and acoustic signal and the known distances (between the sensor and partial discharge source), the acoustic propagation velocity can be calculated. If the velocity is close to acoustic propagation speed in the transformer oil which is 1470 m/s, Then the PD source can be localized. According to the calculations, the velocity is significantly different from 1470m/s. The velocity at three positions is 4170 m/s, 4150 m/s, and 4340 m/s.

The large difference is due to the fact that the PD acoustic signals are transmitted through not only the transformer oil but also the transformer wall which is made of steel. The acoustic speed (about 5000 m/s) in steel is much faster than that in the transformer oil. The detected velocity of about 4250 m/s is smaller than 5000 m/s and larger than 1470 m/s. It shows that the acoustic signals are partly transmitted in the oil and partly in the transformer wall before they arrive at the sensors.

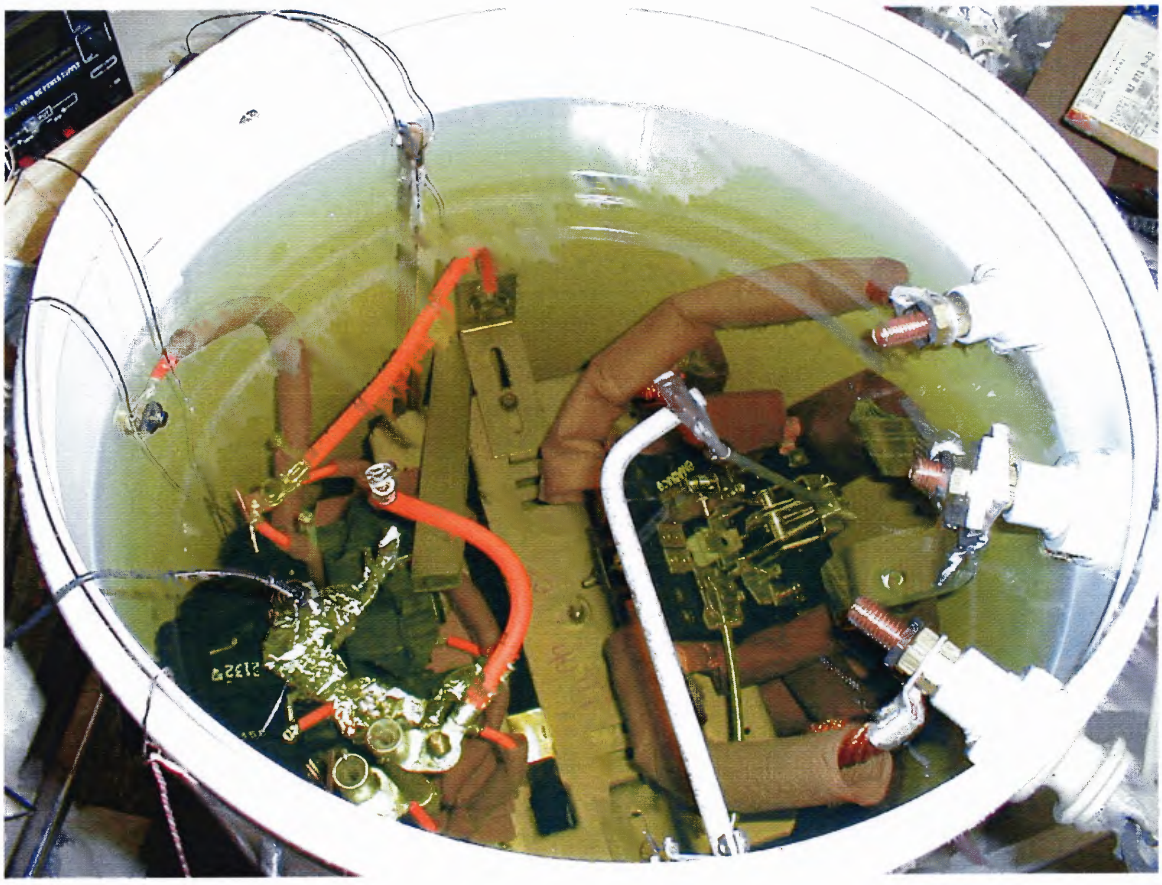

Figure 5.13 The oil filled transformer used in localization experiments.

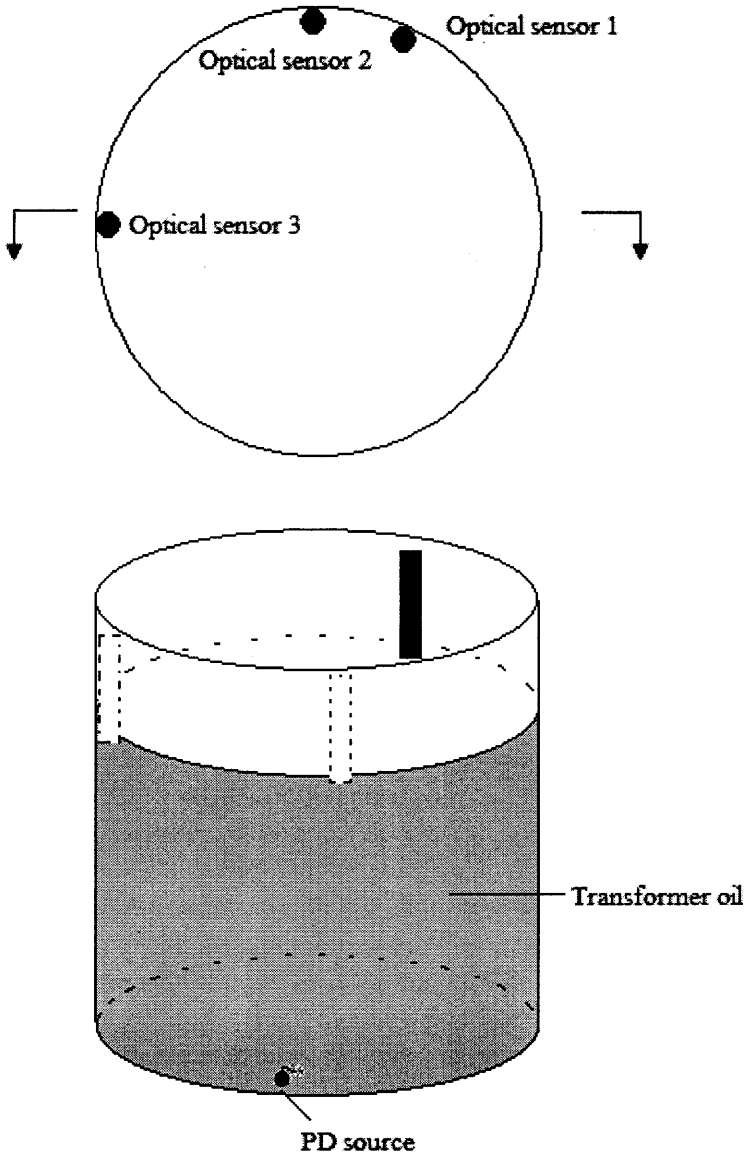

Figure 5.14 Localization setup with the sensor close to the transformer wall.

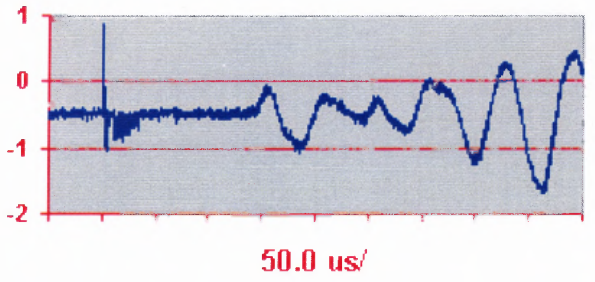

Position 1

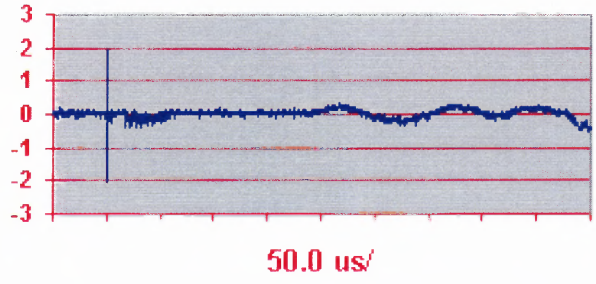

Position 2

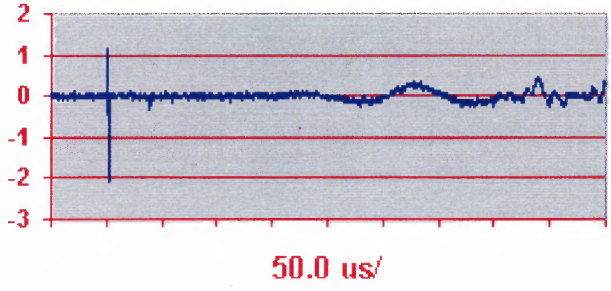

Position 3

Figure 5.15 Experimental results in three positions.

5.4.4 3-D Localization with Sensors in the Center of the Transformer

In the previous experimental setup, the sensor is close to the transformer wall which allows the acoustic signals to transmit in both the transformer oil and transformer wall. In this experiment, the optical sensors are placed near the center of the transformer. Thus the sensors don't touch the transformer wall. In order to make sure there is a same static

pressure applied in the sensors, the optical sensors are in three positions at the same height level of 5 cm below the transformer oil surface. The experimental setup is shown in Figure 5.16. Figure 5.17 shows the sensor outputs in three different positions inside the transformer.

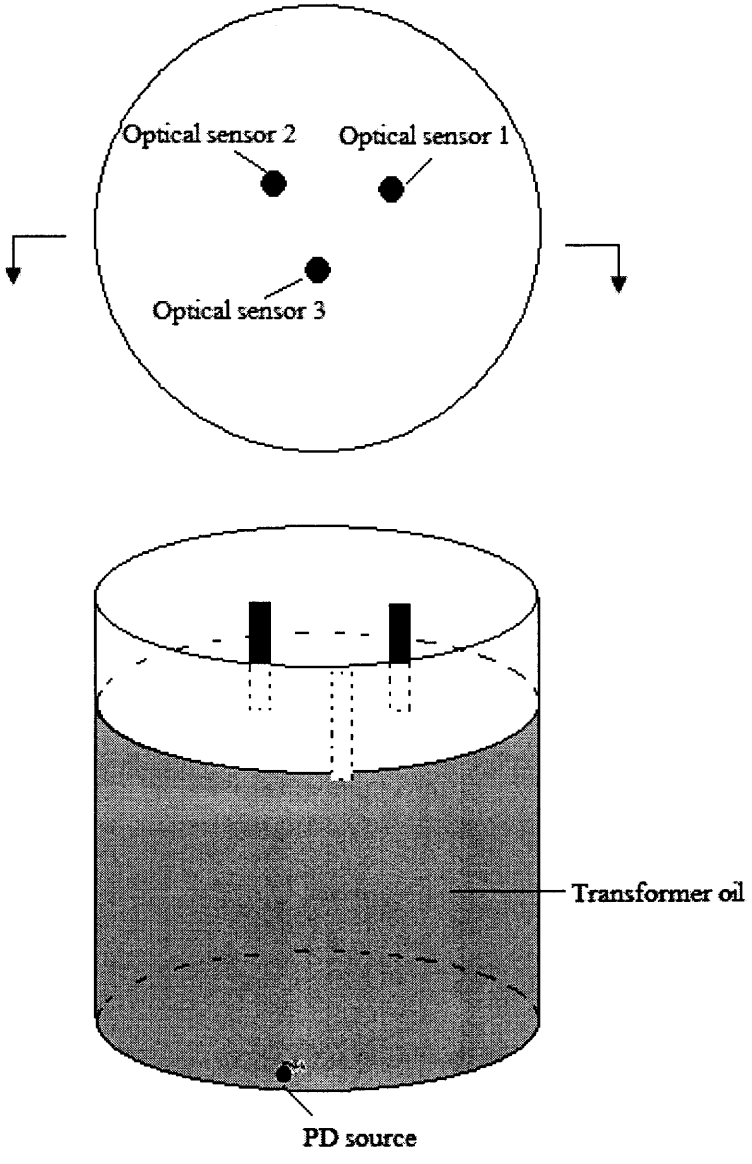

Figure 5.16 Localization setup with the sensor in the center of the transformer.

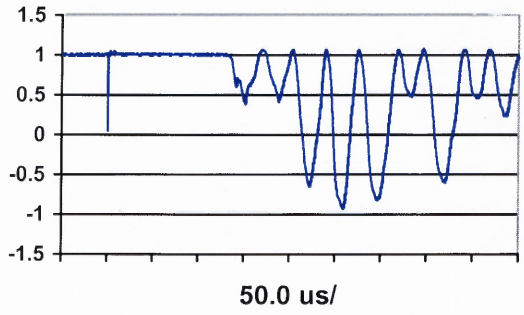

Position 1

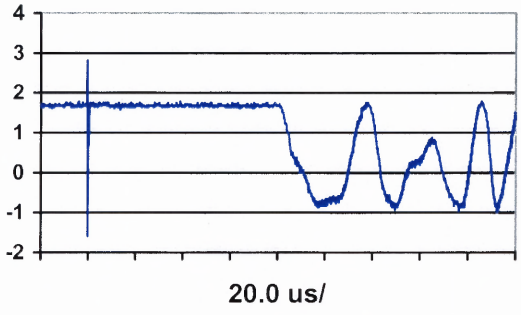

Position 2

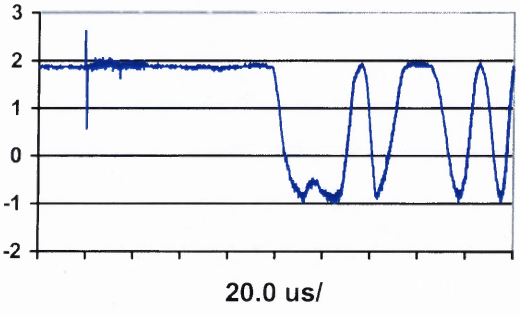

Position 3

Figure 5.17 Experimental results in three positions.

When using the velocity of 1470 m/s in the calculations, the calculation results tell us the partial discharge source is located in (-0.24, 6.9, 30.3). The actual position in the experiment is (0, 7.5, 30). The experimental result is close to the actual position which confirms that the acoustic signals travel only through the transformer oil.

5.4.5 Discussions

Because PD localization is a very important part of PD detection, the localization experiments are conducted in a small tank and a real transformer. When the optical sensors are relatively far from the transformer wall, the detected acoustic signals are mainly transmitted through the transformer oil before they are detected by the optical sensors. The transmission velocity is the acoustic velocity in the transformer oil and it is easy to localize the PD source.

When the sensor is touching or close to the transformer wall, the detected acoustic signals are transmitted through both the transformer oil and wall. This inconsistency yields erroneous results which makes it very difficult to localize the PD source.

CHAPTER 6

CONCLUSIONS AND FUTURE WORK

6.1 Conclusions

Partial discharge (PD) detection and localization in high voltage transformers is an essential diagnostic tool for monitoring the condition of electrical insulators within the transformer. The insulation breaks down over time due to mechanical and electrical stresses and if the insulation damage becomes severe, the device could suffer a catastrophic failure that not only causes an unscheduled service outage, but also causes damage to surrounding equipment and threatens the safety of onsite personnel. Partial discharges are one symptom of insulation breakdown because the developing faults in the insulation cause a local build up of electrical charge, which is then dissipated in the form of an electrical and mechanical pulse of energy. In addition, PDs make insulation damage worse because the event adds more electrical and mechanical stress to the developing flaw. Therefore, accurate detection and positioning is required to maintain these devices and limit the amount of diagnostic and repair time required.

The acoustic wave induced by PD can be measured and used for monitoring, diagnosing, and locating potential failures in power transformers. Optical fiber-based sensors have been shown to be attractive devices for PD detection because of a number of inherent advantages, including small size, high sensitivity, electrical nonconductivity, and immunity to EMI.

The thesis documents the results of a theoretical analysis of PD acoustic signal in transformer oil at different temperatures and compares the results to actual experiments in

the laboratory. The experimental results show that the dominant frequency components in the energy of the PD pulse shift from low frequency to high frequency at increased temperature. A theoretical analysis is shown to be consistent with the experimental results.

The thesis details the development of a fiber optic acoustic sensor system for PD detecting inside the transformer. In principle, the sensor is made according to the principle of a Fabry Perot interferometer. A simple micromachining process compatible with MEMS (Microelectromechanical system) has been developed for fabricating the sensor. A fiber-optic readout scheme has been used to monitor sensor diaphragm deflection. Design, fabrication and characterization are described in the thesis. The resulting sensor has a resolution of 1.6 Pa and a resonant frequency of about 90 kHz.

The sensor used in PD acoustic detection is immersed in oil in a real transformer. The experimental results show that the sensor not only detects the PD signal but also discriminates against the surrounding noises. When the PD localization experiments are conducted in the real transformer and the sensor is not touching or close to the transformer wall, it is easy to localize the partial discharge source. When the sensor is touching or close to the transformer wall, it is very difficult to localize the PD source.

6.2 Future Work

The ultimate goal of this project is to design and implement a PD detection and location system in a commercial power environment. The work presented in this thesis represents the preliminary studies necessary to achieve that goal and demonstrates the feasibility of the approach. First and foremost is the further investigation of the PD phenomenon itself.

It is very important to have the exact, accurate and complete characteristics of acoustic PD pulses including the frequency content and pulse duration. It will also be very helpful to optimize sensor characteristics for detecting the phenomenon.

The second area of future research is an investigation of the effect of obstructions on the propagation of the acoustic waves within the transformer tank. Because of the inhomogeneous nature of the tank, it is important to understand how signals are attenuated and diffracted as they pass through the transformer oil and the transformer wall in the HV transformer. Results of a study of this kind could be used to determine sensor placement within the tank, an efficient sensor layout could be designed to offer the largest coverage of the HV transformer interior with the least number of sensors used to localize the PD source.

The final area of future study is field testing the whole system in a real world HV working transformer. The true accuracy of the system as well as required improvements and optimization can be determined by operating the system under real conditions. The data from such tests would then allow a commercial company to take on the manufacture and installation of this system in HV transformers.

APPENDIX A

SENSOR HOUSING DIMENSIONS

The appendix describes the dimension and structure of the optical sensor housing.

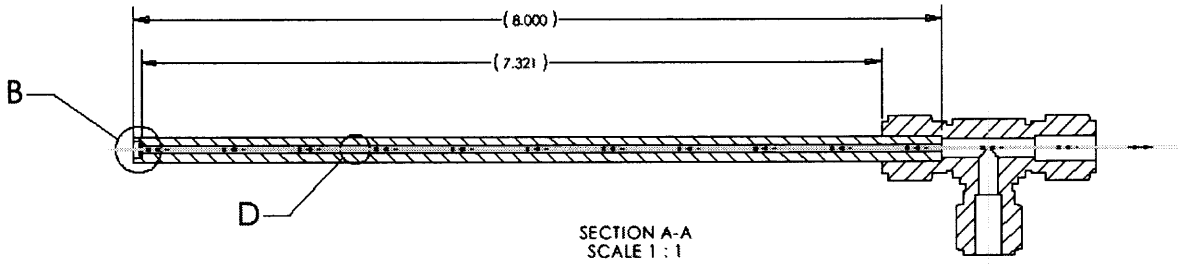

Figure A.1 Optical sensor housing structure and dimensions.

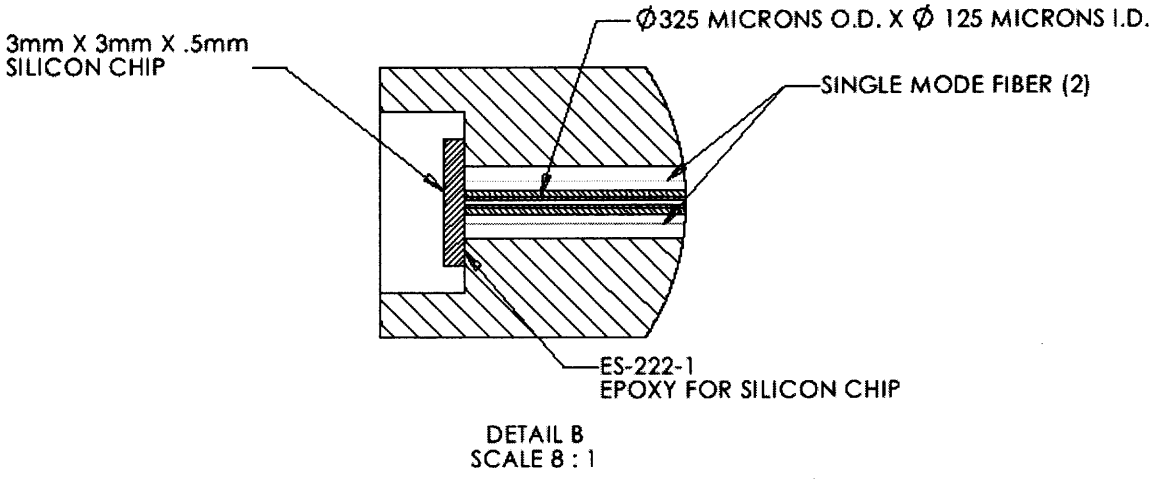

Figure A.2 Detailed dimensions of B in Figure A.1.

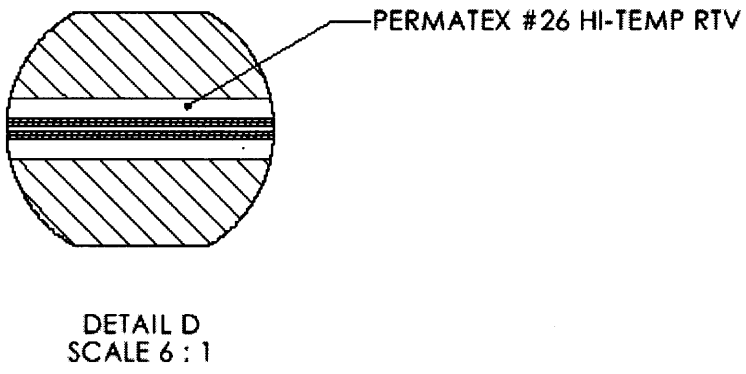

Figure A.3 Detailed demonstration of D in Figure A.1.

APPENDIX B

SILICON WAFER BONDING TRAVELER

This appendix contains the documentation travelers that accompany anodic wafer bonding that uses the Microelectronics Research Center cleanroom facilities at NJIT.

Table B.1 Wafers Anodic Bonding Traveler.

Process	Process Description	Date	Wafer #	Comments
M-Pyrol	Primary bath 95°C, 10 minutes Secondary bath 95°C, 10 minutes Rinse cold DI water 10 minutes Spin dry			
P-clean	5:1 H_2SO_4:H_2O_2 110°C, 10 minutes Hot DI Water 10 minutes Cold DI Water 5 minutes Spin dry			
Oxide Removal	100:1 H_2O:HF 1 minute Rinse 10 minutes Over dry 100°C, 15 minutes			

Steam Oxidation	O_2: 7.5 l/min Bubbler: 530 sccm 1050 °C Target: 3000A			
Measure	Mean: _____Å Std. Dev.: _____Å			
Surface Activation	RCA-2 95°C, 10 minutes Hot DI water rinse 70°C, 5 minutes Cold DI water rinse 5 minutes Over dry 100°C, 15 minutes			
Anodic bonding	Wafer bow Hot chuck to 350°C Temperature Stabilization 10 miniutes Pressure plate down 30 N force Apply voltage 1100 V, 1 minutes Cool down 45 minutes Release pressure plate			

REFERENCES

1. Bartnikas, R. (1990). Detection of partial discharges in electrical apparatus. IEEE Transaction on Electrical Insulation, 25, 111-124.

2. Niemeyer, L. (1995). A generalised approach to partial discharge modeling. IEEE Transaction on Electrical Insulation, 2, 510-528.

3. Nattras, D.H. (1993). The early history of partial discharge research. IEEE Electrical Insulation Magazine, Vol. 9, 27- 31.

4. Kreuger, F. (1989). Partial Discharge Detection in High Voltage Equipment. London: Butterworths Co. Ltd.

5. Bartnikas, R., and McMahon E. J. (1979). Engineering Dielectrics, Corona Measurement and Interpretation. ASTM, STP 669, Philadelphia, U.S.A.

6. Blackburn, T.R. (1998). Acoustic detection of partial discharges using non intrusive optical fibre sensors. IEEE International Conference on Condition and Breakdown in Solid Dielectrics, Vasteras, Sweden.

7. Bartnikas, R. (2002). Partial discharges: their mechanism, detection and measurement, IEEE Transactions on Dielectrics and Electrical Insulation, 9, 763-808.

8. Dawes, C. (1926). Ionization studies in paper-insulated cables I, AIEE Transactions, 45, 141.

9. Robinson, D. (1936). Dielectric Phenomena in HV Cables. London: Chapman and Hall.

10. Bartnikas, R. (1987). A commentary on PD measurement and detection. IEEE Transactions on Electrical Insulation, Vol. El-22, 629-655.

11. Bartnikas, R. (1990). Detection of PD in electrical apparatus. IEEE Transactions on Electrical Insulation, Vol. 25, 111-124.

12. Quinn, G.E. (1940). Detection of the ionization point in electric apparatus. AIEE Transactions, Vol 59, 709-714.

13. Bartnikas, R. and Ombrain, G. (1963). A method for determining the dissipation factor value from corona intensity and pulse count. IEEE Transactions on Power Apparatus and System. Vol. 82S, 366-375.

14. Boggs, S.A. (1990). Partial discharge: overview and signal generation. IEEE Electrical Insulation Magazine, Vol. 6, 33-39.

15. Boggs, S.A. (1990). Partial discharge - part III: cavity-induced PD in solid dielectrics. IEEE Electrical Insulation Magazine, Vol. 6, 11-20.

16. Inoue, Y., Suganuma, K., Kamba, M. and Kikkawa, M. (1990). Development of oil-dissolved hydrogen gas detector for diagnosis of transformers. IEEE Transactions Power Delivery 5, 226-232.

17. Pledger, W.A. and Pyke, S. (1994). Gas monitor update: review of progress in the development of a microelectronic in-situ transformer fault gas analyzer. EPRI Substation Equipment Diagnostics Conference, Electrical Power Research Institute, Palo Alto, California.

18. Abbott, J.W., Chu D., Diamond, A.E. and Slemon, C. (1994). Development of an automated transformer oil monitor (ATOM). EPRI Substation Equipment Diagnostics Conference, Electrical Power Research Institute, Palo Alto, California.

19. Cartlidge, D.M., Casson, D.W., Franklin, D.E., Macdonald, J.A., and Pollock, B.C. (1994). Machine condition monitoring: ozone monitor for air cooled generators. CEA Research Report Contract 9134G864.

20. Kemp, I.J. (1995). Partial discharge plant-monitoring technology: present and future developments. IEE Proc.-Sci. Meas. Technology, Vol. 142, 4-10.

21. Duval, M. (1989). Dissolved gas analysis: it can save your transformer. IEEE Electrical Insulation Magazine, Vol. 5, 22-27.

22. Timperley, J.E. (1983). Detection of insulation deterioration through electrical spectrum analysis. Proceedings of the 16th Electrical/Electronics Insulation Conference, Chicago, Ill., IEEE 83CH1952-1, 60-64.

23. Timperley, J.E. (1983). Incipient fault identification through neutral RF monitoring of large rotating machines. IEEE Transactions on Power Apparatus & Systems, Vol. PAS-102, 693-698.

24. Kheirmand, A., Leijon, M., Hurtig, K., and Väliviita, H. (1997). A system for continuous on-line monitoring and localization of partial discharges in power generators. Proceedings ISH' 97 Montreal, Canada, Vol. 4, 315.

25. Phillipson, J.T. (1996). Experience with RF techniques in the petrochemical industry. 4th International Conference on Generator and Motor Partial Discharge Testing, Houston, Texas.

26. Wichmann, A., Grünewald, P., and Weidner, J. (1987). Early fault detection in electrical machines by on-line RF monitoring. Cigré Sympsium 05-87, Vienna, Austria.

27. Stone, G. (1991). Partial discharge - part VII: practical techniques for measuring PD in operating equipment. IEEE Electrical Insulation Magazine, 7, 9-19.

28. Kawada, H., Honda, M., Inoue, T. and Amemiya, T. (1984). Partial discharge automatic monitor for oil-filled power transformer. IEEE Transactions Power Apparatus System PAS-104, 422-428.

29. Harold, R.T. (1985). Acoustical technology applications in electrical insulation and dielectrics. IEEE Transaction Electrical Insulation, Vol. 20, 3-19.

30. Lundgaard, L. (1991). Acoustic signal propagation from discharge in GIS. Annual Report of the IEEE Conference on Electrical Insulation and Dielectric Phenomena, 91, 449-456.

31. Lundgaard, L. (1992). Partial discharge – part XIV: acoustic partial discharge detection – practical application. IEEE Electrical Insulation Magazine, 8, 34-43.

32. Lundgaard, L. (1992). Partial discharge – part XIII: acoustic partial discharge detection – fundamental considerations. IEEE Electrical Insulation Magazine, 8, 25-31.

33. Varlow, B.R., Auckland, D.W. and Smith, C.D. (1999). Acoustic emission analysis of high voltage insulation. IEE Proc.-Sci. Meas. Technol., Vol. 146, No.5.

34. Harold, R.T. (1979). Acoustic waveguide for sensing and locating electrical discharges in high voltage power transformers and other apparatus. IEEE Transaction PAS-98, No. 2, 449-457.

35. Leijon, M., Ming, L., and Bengtsson, T. (1992). PD-source identification in solids. IEEE Seminarian, Baltimore, MD, 15-418.

36. Lazarevich, A.K. (2003). Partial discharge detection and localization in high voltage transformers using an optical acoustic sensor. The Virginia Polytechnic Institute and State University Master Thesis.

37. Harold, R.T. (1976). The relationship between ultrasonic and electrical measurements in oil corona sources. IEEE Transaction Electrical Insulation Vol. EI-11, No. 1, 8-11.

38. Ogihara, H. (1964). Detection and location of coronas in oil-immersed transformer with corona detector. Electrical Engineering Japan, Vol. 84, 12-22.

39. Blackburn, T.R. (1993). Optical fiber sensor for partial discharge detection and location in high-voltage power transformer. Sixth International Conference on Dielectric Materials, Measurements and Applications, Manchester, U.K.

40. Zhao, Z. and Demokan, M. (2000). The directionality of an optical fiber high-frequency acoustic sensor for partial discharge detection and location. Journal of Lightwave Technology, Vol. 18, 795-806.

41. Zhao, Z. and Demokan, M. (1996). Optical fiber acoustic sensor for sensing and locating partial discharges in high-voltage oil-filled power transformers. 21st Australia Conference on Optical Fiber Technology, Gold Coast, Australia.

42. Blackburn, T.R., Krcho, D. and Zargari, A.(1994). Modified optical fiber sensor for partial discharge detection in high-voltage power transformer. Australia University Power Engineering Conference, Adelaide, Australia, 417-442.

43. Deng, J., Huo, W., Luo, M., May, R., Wang, A., and Liu, Y. (2001). Optical fiber sensor-based detection of partial discharges in power transformers. Optics and Laser Technology, Vol. 33, 305-311.

44. Boggs, S. (1994). Partial discharge – part II: detection sensitivity. IEEE Electrical Insulation Magazine, 6, 34.

45. Boggs, S. (1991). Optimum electrical PD test method for large capacitor. IEEE Transaction Electrical Insulation, 26, 479.

46. Haeren, V., Stone, G. and Kurtz, M. (1985). Preventive failure in outdoor distribution- class metal-clad switchgear. IEEE Transaction PAS, 2706.

47. Harold, R.T. (1985). Acoustical Technology Applications in Electrical Insulation and Dielectrics. IEEE Transaction Electrical Insulation, Vol. 20, No.1, 3-19.

48. Skubis, J. (2003). The application of acoustic emission to estimate partial discharges occurring in transformers and transformer bushings. Proceedings of 5th international symposium on High Voltage Engineering, Baunscheig, 1987.

49. Unsworth, J. (1994). On-line partial discharge monitor for high voltage power transformers. Proceedings of the 4th International Conference on Properties and Applications of Dielectrics Materials, Brisbane, Australia.

50. Sakoda, T. (1999). Analysis of acoustic emissions caused by the PD in the insulation oil. Proceedings of 13th International Conference on Dielectric Liquids, Japan, 483-486.

51. Sakoda, T., Arita, T., Nieda, H. and Ando K. (1999). Acoustic emission caused by the corona discharge in an oil tank. High Voltage Engineering Symposium, 5164-5167.

52. Howells, E. (1984). Parameters affecting the velocity of sound in transformer oil. IEEE Trans. Power Apparatus and Systems, Vol. 103, No.5, 1111-1115.

53. Kinsler, L.E. and Frey A.R. (1982). Fundamentals of Acoustics. Academic Press, John Wiley & Sons.

54. http://www.76lubricants.com/index.htm, retrieved in September 2002.

55. Douglas, J.F. and Gasiorek, J.F. (1979). Fluid Mechanics. Pitman Publishing, UK.

56. Zheng, D. (1988). The study of acoustic emission method for detection of PDs in power transformers. IEEE Trans. Electrical Insulation, Vol. 2, Peking, China, 614-617.

57. Por, G. (1989). Detecting PD in HV measuring transformers by noise method. 6th Symposium on Technical Diagnostics, Prague, Czechoslovakia, 521-524.

58. Culshaw, B. (1988). Basic concepts of optical fiber sensors. Optical Fiber Sensors: Principles and Components, Boston.

59. Halg, B. (1992). A silicon pressure sensor with a low-cost contactless interferometric optical readout. Sensors and Actuators, 30, 225-229.

60. M. Chan, S. Collins, and R. Smith (1994). A micromachined pressure sensor with fiber-optic interferometric readout. Sensors and Actuators, 43, 196-201.

61. Aratani, K., French, P., Sarro, P. and Middlehoek, S. (1994). Surface micromachined tunable interferometer array. Sensors and Actuators, 43, 17-23.

62. Bucaro, J.A., Dardy, H.D. and Carome, E. (1977). Fiber optic hydrophone. Journal of the Acoustical Society of America, 62, 1302-1304.

63. Dandridge, A. and Kersey, A.D. (1995). Overview of Mach–Zehnder sensor technology and applications. Fiber Optic Sensors, Vol. MS 108 of SPIE Milestone Series, Bellingham, Washington, 216-234.

64. Gunther, M.F., Wang, A., Murphy, K.A. and Claus, R.O. (1992). Fiber optic impact detection and location system embedded in a composite material. Fiber Optic Smart Structures and Skins V, Proc. SPIE 1798, 262-270.

65. Greene, J. A., Tran, T.A., Bhatia, V., Gunther, M.F., and Claus, R.O. (1995). Optical fiber sensing technique for impact detection and location in composites and metal specimens. J. Smart Mater. Struct. 4, 93-99.

66. Furstenau, N., Schmidt, M., Horack, H., Goetze, W. and Schmidt, W. (1997). Extrinsic Fabry–Perot interferometer vibration and acoustic sensor systems for airport ground traffic monitoring. IEE Proc. Optoelectron. 144, 134-144.

67. Teunissen, J., Helmig, C., Merte, R. and Peier, D. (2001). Fiber optical on-line monitoring for high-voltage transformers. SPIE International Symposium on Environmental and Industrial Sensing, Proc. SPIE 4204, 198-205.

68. Dakin, J., Wade, C. and Withers, P. (1987). An optical fiber pressure sensor. SPIE Fiber Optics'87, Fifth International Conference on Fiber Optics and Opto-electronics, 734, 194-201.

69. Angelidis, D. and Parsons, P. (1992). Optical micromachined pressure sensor for aerospace applications. Opt. Eng., Vol. 31, 1638-1641.

70. Mendez, T. and Ramsey, K.A. (1993). Micromachined Fabry–Pérot interferometer with corrugated silicon membrane for fiber optic sensing applications. Proc. SPIE—Int. Soc. Optical Engineering, Vol. 1793, 170-182.

71. Kim, Y. and Neikirk, D.P. (1995). Micromachined Fabry–Perot cavity pressure transducer. IEEE Photonics Technology Letter, Vol. 7, 1471-1473.

72. Han, J. and Neikirk, D.P. (1996). Deflection behavior of Fabry-Perot pressure sensors having planar and corrugated membrane. SPIE's Micromachining and Microfabrication '96 Symposium:Micromachined Devices and Components II, R. Roop and K. Chau, Proc. SPIE 2882, Austin. 79-90.

73. Pinnock, R.A. (1998). Optical pressure and temperature sensors for aerospace applications. Sensor Review, Vol. 18, 32-38.

74. Beggans, M.H., Ivanov, D.I., Digges, T.G., and Farmer, K.R. (1999). Optical pressure sensor head fabrication using ultra-thin silicon wafer anodic bonding. Proc. SPIE—Int. Soc. Optical Engineering., Vol. 3680, 773-782.

75. Han, J. (1999). Novel fabrication and characterization method of fabry-perot microcavity pressure sensors. Sensors and Actuators, 75, 168-175.

76. Gander, M.J., MacPherson, W.N., Stevens, R. and Jones, T.V. (2003). Embedded micromachined fiber-optic Fabry-Perot pressure sensors in aerodynamics applications, IEEE Sensors Journal, Vol. 3, 102-107.

77. Heavens, O.S. (1955). Optical Properties of Thin Solid Films. Butterworths Scientific Publications, US.

78. Jerman, J. (1990). The fabrication and use of micromachined corrugated silicon diaphragm. Sensors and Actuators, A21-A23, 988-992.

79. Timoshenko, S. and Woinowsky, S. (1959). Theory of Plates and Shells, McGraw-Hill, New York, 404.

80. Mehregany, M. (1986). Application of micromachined structures to the study of mechanical properties and adhesion of thin films. Master Thesis, MIT, 51-108.

81. Giovanni, M.D. (1982). Flat and Corrugated Membrane Design Handbook. Mercel Dekker Inc., New York.

82. Morse, P.M. and Ingard K.U. (1968). Theoretical Acoustic. New York: McGraw-Hill, 209-222.

83. Harrays, C.M. (1966). Shock and Vibration Handbook. New York: McGraw-Hill, 7.38-7.45.

84. Obermeier, E. (1995). Anodic wafer bonding. Semiconductor Wafer Bonding: Physics and Applications III, Electrochemical Society Proceedings 95-7, New Jersey, 212-220.

85. Gösele, U. and Stenzel, H. (1995). A short history of wafer bonding. Semiconductor Wafer Bonding: Physics and Applications III, Electrochemical Society Proceedings 95-7, New Jersey, 33-46.

86. Madou, M. (1997). Fundamentals of Microfabrication. 384-393.

87. Nese, M. (1993). Anodic bonding of silicon to silicon wafers coated with aluminum, silicon dioxide, polysilicon or silicon nitride. Sensors and Actuators A., 37-38, 61-67.

88. Darley, V. (1991). Partial discharges within power transformers and the use of ultrasonic techniques in their location. IEE Colloquium on Assessment of Degradation Within Transformer Insulation Systems.

89. Murphy, K.A., Gunther, M.F., Wang, A. and Claus, R.O. (1994). Detection of acoustic emission location using optical fiber sensors. Smart Structures and Materials Proc. SPIE 2191, 282-290.

90. Yu, B., Deng, J., Xiao, H., and Wang, A. (2003). Fiber Fabry–Perot sensors for detection of partial discharges in power transformers. Applied Optics, Vol.43, 3241-3250.